Cell Reports Methods

CellPress
OPEN ACCESS

Perspective

# Elucidating the spatiotemporal dynamics of glucose metabolism with genetically encoded fluorescent biosensors

Xie Li,[1,2,3,*] Xueyi Wen,[2,3] Weitao Tang,[1,3] Chengnuo Wang,[1] Yaqiong Chen,[1] Yi Yang,[1] Zhuo Zhang,[1,2,*] and Yuzheng Zhao[1,2,*]

[1]Optogenetics & Synthetic Biology Interdisciplinary Research Center, Shanghai Frontiers Science Center of Optogenetic Techniques for Cell Metabolism, State Key Laboratory of Bioreactor Engineering, School of Pharmacy, East China University of Science and Technology, 130 Mei Long Road, Shanghai 200237, China

[2]Research Unit of New Techniques for Live-Cell Metabolic Imaging, Chinese Academy of Medical Sciences, Beijing 100730, China

[3]These authors contributed equally

*Correspondence: xieli@ecust.edu.cn (X.L.), zhangzhuo@ecust.edu.cn (Z.Z.), yuzhengzhao@ecust.edu.cn (Y.Z.)

https://doi.org/10.1016/j.crmeth.2024.100904

## SUMMARY

Glucose metabolism has been well understood for many years, but some intriguing questions remain regarding the subcellular distribution, transport, and functions of glycolytic metabolites. To address these issues, a living cell metabolic monitoring technology with high spatiotemporal resolution is needed. Genetically encoded fluorescent sensors can achieve specific, sensitive, and spatiotemporally resolved metabolic monitoring in living cells and *in vivo*, and dozens of glucose metabolite sensors have been developed recently. Here, we highlight the importance of tracking specific intermediate metabolites of glycolysis and glycolytic flux measurements, monitoring the spatiotemporal dynamics, and quantifying metabolite abundance. We then describe the working principles of fluorescent protein sensors and summarize the existing biosensors and their application in understanding glucose metabolism. Finally, we analyze the remaining challenges in developing high-quality biosensors and the huge potential of biosensor-based metabolic monitoring at multiple spatiotemporal scales.

## INTRODUCTION

Glucose is one of the major nutrients in all living organisms, and the underlying metabolic mechanism was elucidated many years ago. Glucose is oxidized via glycolysis and the pentose phosphate pathway (PPP) (Figure 1). During glycolysis, glucose breaks down into pyruvate, coupling with the formation of adenosine triphosphate (ATP) and nicotinamide adenine dinucleotide (NADH). Furthermore, lactate dehydrogenase converts pyruvate into lactate and NADH to $NAD^+$, resulting in no net production of NADH from glycolysis. The PPP generates the nucleotide precursor ribose-5-phosphate and the fundamental reducing equivalent NADPH (NADH phosphate). In addition, glucose can be used to synthesize glycogen for energy storage and, alternatively, serve as substrates for the glycosylation of proteins through the hexosamine biosynthetic pathway or directly added to lipids for glycosylation. Glucose can be acquired through dietary uptake or synthesized via the gluconeogenesis pathway. In mammals, under physiological conditions, gluconeogenesis mainly occurs by using the substrates of pyruvate, glucogenic amino acids, and glycerol in the liver and, to a lesser extent, the kidney and intestine.

Commonly used sugars other than glucose comprise monosaccharides, which include fructose and galactose, and disaccharides, such as sucrose, maltose, lactose, and trehalose (Figure 1). When these disaccharides undergo hydrolysis to monosaccharides, the monosaccharides may enter the glycolytic pathway at several points, and galactose are often consumed in the glycosylation pathway.

## BIOLOGICAL FUNCTIONS OF GLUCOSE METABOLITES

Glucose metabolism plays vital roles in both prokaryotic and eukaryotic cells. It supplies energy and biomass building blocks while also regulating redox homeostasis by determining the two critical redox parameters, NADH/$NAD^+$ and NADPH/$NADP^+$. Additionally, glucose serves as the substrate for glycosylation, which is one of the most abundant posttranslational modifications.[1] Large-scale studies have identified thousands of interactions between metabolites and proteins.[2–4] While many of these interactions have not been fully explored, numerous interactions mediated by glycolytic metabolites have been shown to have important biological effects. The end product of glycolysis, lactate, can bind directly to the mitochondrial signaling adaptor protein MAVS and thereby prevent MAVS aggregation and impede interferon production in antiviral immunity.[5] Lactate also binds to and inhibits the SUMO protease SENP1, which triggers the degradation of the anaphase-promoting complex and exit

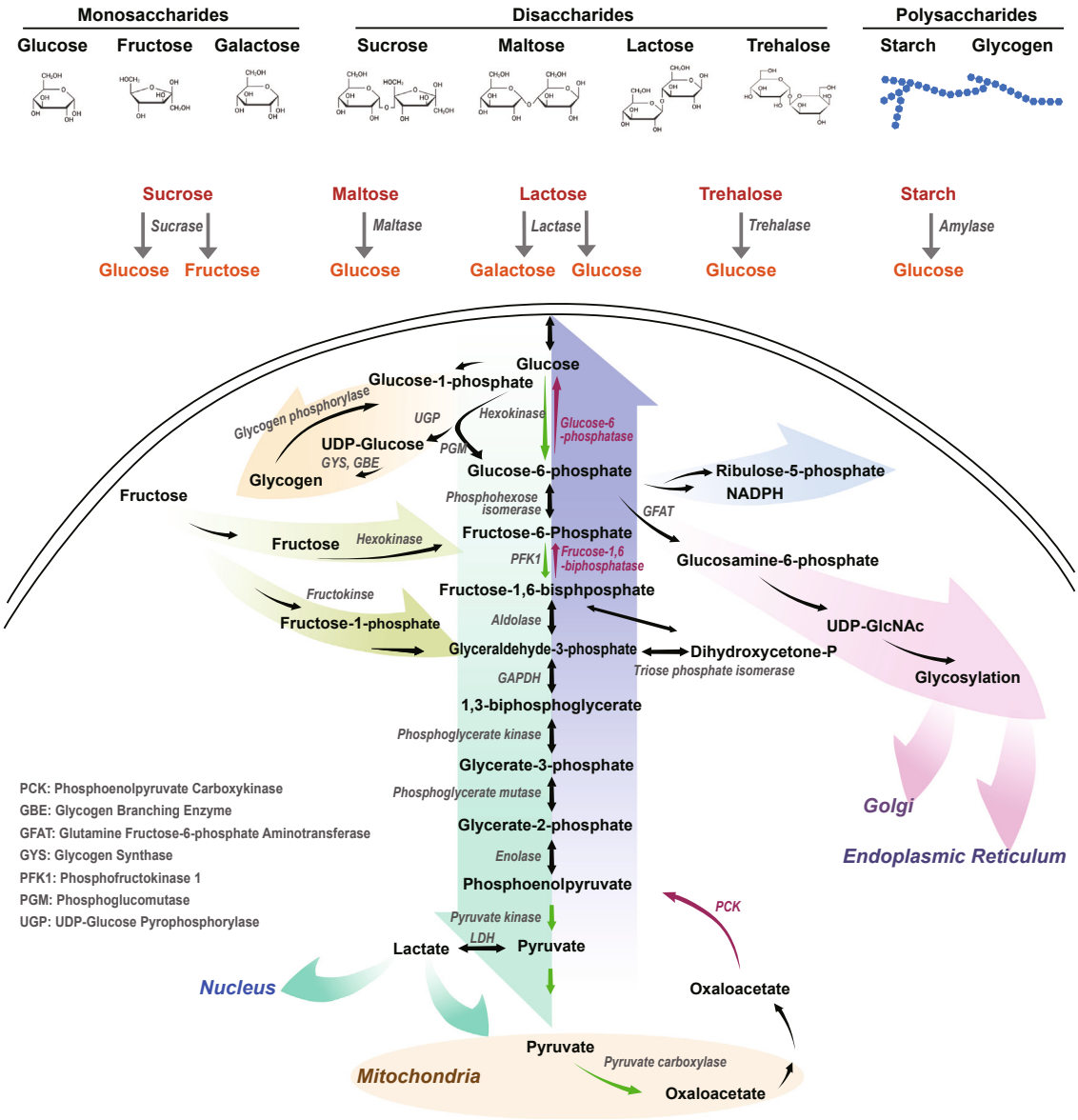


**Figure 1. Metabolic pathways for glucose and other saccharides**

Glucose can be catabolized through the glycolytic pathway (green) and the pentose phosphate pathway (blue), utilized in glycosylation (pink), and stored as glycogen (yellow). Intracellular glucose comes from dietary uptake or gluconeogenesis (blue-purple). Glycogen and disaccharides are hydrolyzed to monosaccharides, and the monosaccharides then enter the glycolytic pathway or are directly utilized (e.g., for glycosylation).

from mitosis in proliferative human cells.[4] Furthermore, lactate can act as the substrate for lactylation, a type of posttranslational protein modification, and therefore has important effects on the activities of cytoplasmic and nuclear proteins.[6–8] Other important glycolytic intermediates, such as dihydroxyacetone phosphate (DHAP) and phosphoenolpyruvate (PEP), also possess functions beyond cellular metabolism. In the cytosol, DHAP and, to a much lesser extent, glyceraldehyde-3-phosphate mediate the sensing of glucose availability through the activation of the mTORC1 signaling complex[9]; in the nucleus, DHAP eliminates acetate by generating 1-acetyl-DHAP and therefore prevents global histone acetylation during cell cycling.[10] In helper T cells, PEP suppresses the activity of SERCA, a $Ca^{2+}$-ATPase that transports cytosolic calcium ions into the endoplasmic reticulum, thereby sustaining $Ca^{2+}$-mediated signaling and supporting T effector functions.[11] Collectively, these studies illustrate the varied functions of glycolytic intermediates beyond cellular metabolism and highlight the need to monitor specific glucose metabolites.

## SPATIAL DISTRIBUTION OF GLYCOLYTIC METABOLITES

Glucose metabolism has generally been thought to occur in the cytoplasm, comprising glycolysis, the PPP, and major reactions

of gluconeogenesis. The transformation of pyruvate into PEP, which is a rate-limiting step for gluconeogenesis, can take place in either mitochondria or the cytoplasm. Nevertheless, the conventional notion that glycolytic intermediates are uniformly distributed throughout the cytoplasm has been challenged. First, various types of protein granules comprising glycolytic enzymes have been identified in the cytoplasm. This finding suggests that glucose metabolism can occur locally within a small cytoplasmic volume, giving rise to a transient fluctuation in the spatial distribution of glycolytic intermediates. Second, an increasing body of evidence indicates that glycolytic metabolites may also be located in the nucleus and mitochondria, where they carry out important functions.

### Compartmentation in organelles

All essential glycolytic enzymes and some metabolic enzymes in the tricarboxylic acid (TCA) cycle have been found in the nucleus, in addition to glucose transporters in the nuclear envelope.[12,13] These observations suggest that glycolysis may be active in the nucleus. Indeed, the oxidation of pyruvate to acetyl-coenzyme A (CoA) by nuclear pyruvate dehydrogenase offers an essential substrate for histone acetylation and is involved in cell cycle progression and likely the epigenetic remodeling that occurs during zygotic genome activation.[14,15] Lactate is necessary for histone lactylation, which regulates gene expression,[7] and MRE11 lactylation, which regulates the DNA repair process.[8] In addition, $NAD^+$ is consumed for the modification of both histones and nucleic acids; histone ADP-ribosylation is important for DNA repair,[16] and the capping of mRNA at the 5′ end with $NAD^+$ has been shown to modulate the stability of mRNAs.[17] Competition for $NAD^+$ between the nucleus and cytoplasm has been shown to play an essential role in adipocyte differentiation.[18] Alternatively, there is a possibility that $NAD^+$ regeneration during the reduction of pyruvate to lactate facilitates these $NAD^+$-consuming processes, but this has not yet been investigated. Compared to the metabolite transport between subcellular compartments, the local production of essential metabolites is likely efficient when the metabolites are chemically active and unstable in cells.

In addition to the nucleus, other organelles also contain glycolytic metabolites. A lactate sensor study showed that mitochondria in mammalian cells were enriched with 5-fold more lactate than in the cytoplasm, as will be discussed in more detail later.[19] A comparably abundant pool of lactate also appeared in the endoplasmic reticulum, although its function remains elusive.[20] In addition, fructose-1,6-bisphosphate has been reported to mediate the Crabtree effect, which describes the inhibition of oxidative phosphorylation by active glycolysis, both in isolated mitochondria and living cells.[21,22] This finding implies that fructose-1,6-bisphosphate may be present in mitochondria, but conclusive evidence is still lacking.

### Compartmentation in protein granules

There is emerging evidence that at least some of the glycolytic enzymes are not homogeneously diffused throughout the cytoplasm and that their locations have important biological consequences; for example, glucose-6-phosphate favors the glycolytic pathway when the hexokinase HK1 associates with mitochondria in macrophages, whereas it favors the PPP over glycolysis when HK1 associates with some members of the cytosolic S100 protein family.[23] Enzymes involved in glucose metabolism are organized into membraneless granules in the cytoplasm. One type of complex, called the glucosome, contains four glycolytic and gluconeogenic enzymes. In response to metabolic and signaling manipulation, glucosomes display different sizes and switch metabolic activities from glycolysis to the PPP to serine biosynthesis in normal and cancer cells.[24,25] Another complex, called the glycolytic body (G-body), is formed under hypoxia in yeast and cancer cells, and it contains various metabolic enzymes, with phosphofructokinase serving as a critical component.[26] G-body formation is correlated with increased levels of glycolytic intermediates and decreased levels of metabolites in the PPP. Similar granules appear in the synapses of *C. elegans* neurons in response to energy stress, and glycolysis is necessary to sustain synaptic activity and locomotion.[27] In addition, glycolysis is closely linked to cytoskeletal architecture. As the primary energy-producing process in the cytoplasm, glycolysis may support the energetically costly activity of cytoskeletal remodeling. Mechanistically, mechanical stress stimulates the recruitment of the glucose transporter GLUT1 to junctions between epithelial cells, and increased glucose metabolism can strengthen the actin cytoskeleton and contribute to epithelial barrier formation.[28] Alternatively, glycolytic enzymes are translocated into the lamellipodia and cell protrusions of endothelial tip cells to support angiogenesis.[29] Conversely, cytoskeletal organization exerts a rapid effect on glycolytic activity; for example, aldolase localized in the actin cytoskeleton is inactive, whereas disassembly of actin cytoskeleton may release the enzymes into the cytoplasm and thus increase glycolytic flux.[30]

## GENETICALLY ENCODED FLUORESCENT SENSORS FOR GLYCOLYTIC METABOLITES

Glucose metabolites can be measured by several techniques. As the mainstay techniques, chromatography, mass spectrometry, and nuclear magnetic resonance are commonly used to measure multiple glucose metabolites simultaneously. The enzymatic cycling assay is an alternative assay to assess glucose metabolites. Cells and tissue samples are usually lysed during metabolite sample preparation, thereby losing information about the spatiotemporal dynamics of metabolites in living cells and organisms. Positron emission tomography with the radiolabeled glucose analog $^{18}$F-FDG is used to track the glucose uptake for diagnostic purposes, and fluorescently labeled glucose analogs have also been developed for research purposes, but these molecules generally cannot be metabolized as glucose in living cells, so they indicate only the glucose uptake, not the levels of intermediates and end products. Seahorse analyzer technology is increasingly being used to analyze bioenergetics in living cells by measuring the extracellular acidification rate and oxygen consumption rate; however, it cannot be applied to monitor glucose metabolites at the single-cell or subcellular resolution or *in vivo*.

### Introduction to genetically encoded fluorescent sensors

Genetically encoded fluorescent sensors are emerging as a powerful tool for metabolic analysis. A major advantage of the

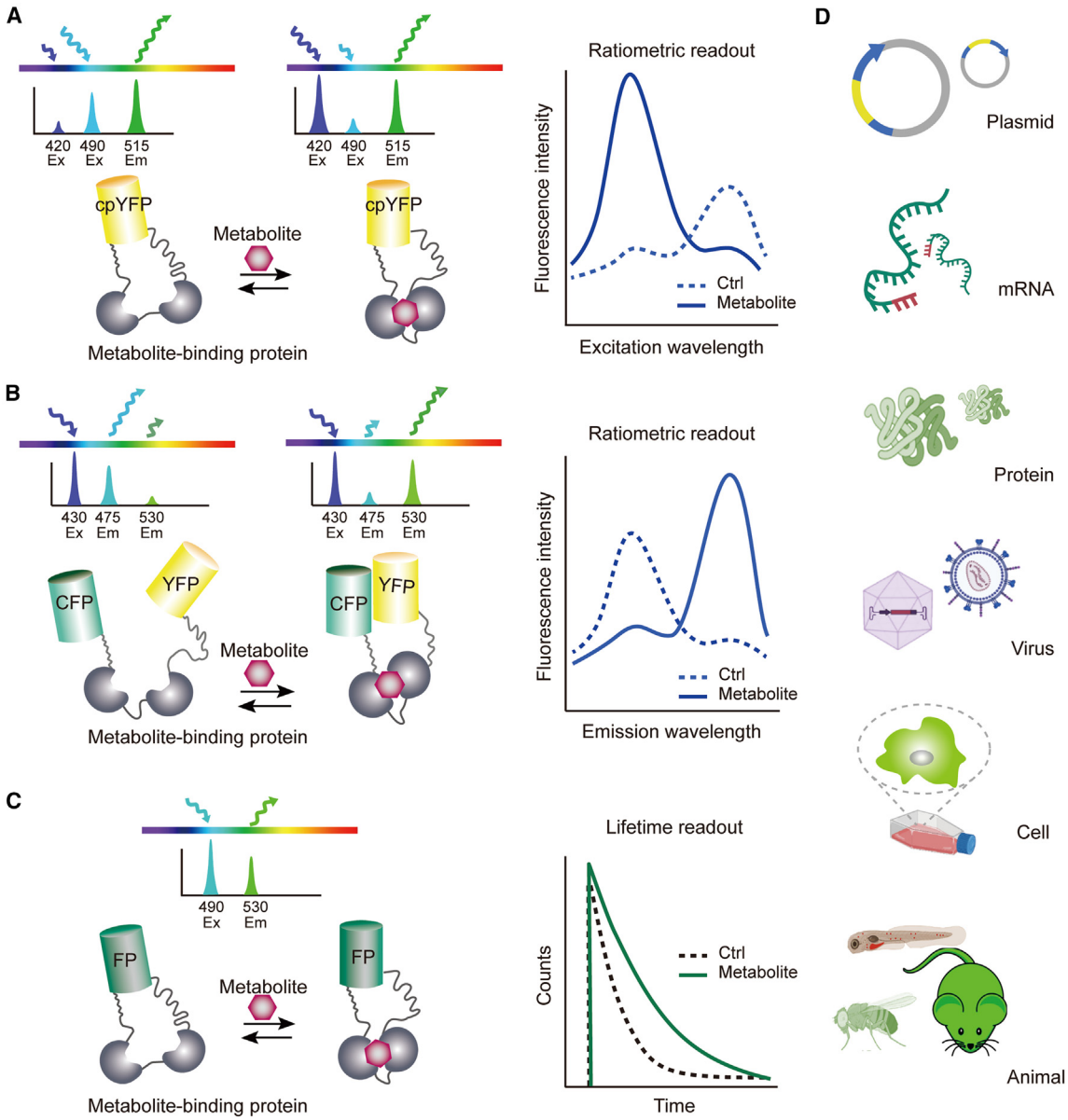


**Figure 2. Genetically encoded fluorescence sensors for glucose metabolites**

(A–C) Biosensors are designed as two types, single FP type (A) and FRET type (B), and their fluorescent readouts are based on measuring either intensity (A and B) or lifetime of fluorescence (C). The readouts of FRET-type sensors are naturally ratiometric, single-FP-type sensors can have either a ratiometric or intensiometric readout, and both types of sensors may have the lifetime readout.

(D) Delivery and expression of sensors can be achieved via numerous ways, including transduction of plasmid/viral vectors/mRNA carrying sensor-coding sequences, injection of purified sensor proteins, transplant of cell lines with stable sensor expression, and transgenic expression.

genetically encoded biosensors is their ability to enable the spatiotemporal monitoring of metabolite dynamics in live animals, which cannot be achieved by other measurement strategies like mass spectrometry and Seahorse analyzer. Since metabolite pools often sensitively respond and timely adapt to the intracellular regulatory processes and extracellular environmental changes, and real-time metabolic monitoring *in situ* would offer valuable insights, particularly in living organisms under natural conditions, which cell culture may not mimic well. These biosensors can be designed as fluorescent protein (FP) sensors, fluorescent RNA sensors, semisynthetic fluorescent sensors with self-labeled protein tags, or bioluminescent sensors. The latter three types of sensors cannot self-sufficiently form intrinsic fluorophores alone; thus, exogenous dyes or chemicals are needed. The handling of exogenous substances, such as incubation and washing off excess chemicals, is time consuming and makes the assay susceptible to artifacts. In contrast, FP sensors have intrinsic fluorescence and are more

convenient and powerful tools. FP sensors are classified into two types (Figures 2A and 2B). One type, based on the principle of fluorescence energy resonance transfer (FRET), is usually constructed by linking a metabolite-binding protein to a FP FRET pair, and binding to metabolites then induces a change in FRET efficiency. The other type, which we refer to here as the single FP type, is constructed by fusing a single FP with a metabolite-binding protein so that the conformational change upon binding to a metabolite may induce a shift in the fluorescence spectrum of the biosensor.

For both FRET-type and single-FP-type sensors, metabolite binding is expected to trigger a conformational change in the sensor, resulting in a shift in FRET efficiency or the fluorescence spectrum, respectively. Both original FPs and their variants, circularly permutated FPs (cpFPs), are used for engineering sensors.[31] cpFPs are created by sealing the original protein N and C termini and opening new termini near the fluorophore, which sometimes make the proteins more sensitive to conformational changes. The fluorescence readout can be either fluorescence intensity or fluorescence lifetime. Fluorescence intensity is commonly used and can be conveniently measured using routine instruments such as fluorescence microscopes, flow cytometers, and plate readers. If the fluorescence spectra have two excitation wavelengths (e.g., cpYFP based) or emission wavelengths (e.g., FRET type), then the ratio of fluorescence values between the two peaks can be used as a readout. This readout is independent of the absolute fluorescence intensity, thus eliminating the influence from expression levels of sensors in cells and excitation intensity (Figures 2A and 2B). The fluorescence lifetime, which is the average time between the absorption and emission of a photon, also provides a robust readout (Figure 2C). However, this method requires sophisticated instrumentation and data processing and is therefore less commonly used in general laboratories.

Numerous ways have been established for FP sensors to be delivered and expressed in live cells and organisms (Figure 2D). Plasmids and viral vectors carrying sensors' coding sequences are commonly used for sensor expression in live cells. For transient expression, sensor proteins or sensor-coding mRNAs can be used to deliver cells of interest. Expression *in vivo* can be achieved through the transplantation of sensor-expressing cells, electroporation, adeno-associated viruses, or transgenic technology.

## Glucose metabolite sensors

Dozens of genetically encoded fluorescent sensors have now been developed to monitor glucose metabolism (Figure 3). These sensors can be classified into three classes based on the substrates they detect, including (1) monosaccharides, disaccharides, and their metabolites, (2) pyridine dinucleotides as essential coenzymes, and (3) the energy currency ATP and its derivatives.

Biosensors for pyridine dinucleotides constitute a relatively complete toolkit. Commonly used sensors include the $NAD^+$ sensors LigA-cpVenus[32] and FiNad,[33] the NADH sensor Frex,[34] the $NAD^+$/NADH sensors SoNar[35,36] and Peredox,[37] the $NADP^+$ sensor Apollo-$NADP^+$,[38] and the NADPH sensor iNap family,[39,40] while a high-quality (high specificity, high responsiveness, appropriate affinity, ratiometric readout, rapid response, etc.) sensor for $NADP^+$/NADPH is lacking. The available energy currency reporters are the ATP sensors ATeam,[41] AT1.03NL,[42] iATPSnFR,[43] $GRAB_{ATP1.0}$,[44] and MaLion[45] and the ATP/$ADP^+$ sensor Perceval[46] and its modified version PercevalHR.[47] As all these sensors have been summarized in a previous review article,[48] we will focus here on the class of sensors for specific glucose metabolites (Table 1).

### *Sensors for glucose*

The FLIPglu glucose sensors have been established and continuously optimized. FLIPglu-600μ, the original, was constructed by linking the *E. coli* glucose/galactose-binding protein MglB with a FRET pair, CFP and YFP, and had an apparent dissociation constant ($K_D$) of 590 μM for glucose.[49] This sensor responded to glucose and galactose with comparable affinity. A screen performed to optimize the insertion site in MglB and the linker sequence resulted in a few variants with $K_D$ values for glucose ranging from ∼0.6 to ∼13.8 mM. Among them, the $FLII^{12}Pglu$-600μ sensor showed a fluorescent ratio response of 58% *in vitro* and an apparent $K_D$ of 600 μM.[50] Further mutant screening based on $FLII^{12}Pglu$-600μ generated five sensors, and $FLII^{12}Pglu$-700μδ6 exhibited the best performance, with a $K_D$ of 600 μM in cells and a dynamic response of 74%.[51] These glucose sensors have been used for the real-time monitoring of glucose dynamics in yeast, mouse, and human cells.[51,74,75] Another family of glucose sensors (we refer to as gT112M37 in Table 1) was constructed with a similar design strategy to that of the FLIPglu family by fusing the *E. coli* MglB protein with a FRET pair, ECFP and Venus, and they showed a 15%–35% fluorescent response to glucose and apparent $K_D$ values of 0.3–284 μM.[52] The sensor GIP, engineered by fusing a FRET pair, $GFP_{\mu\nu}$ and YFP, with the periplasmic glucose-binding protein (GBP), exhibited a 20% change in fluorescent ratio upon binding to glucose and an apparent $K_D$ for glucose of ∼5 μM[53]

All of the above sensors are FRET-type sensors, but a few single-FP-type sensors have been developed in the past several years. The glucose sensor named FGBP was designed by inserting cpYFP into the *E. coli* MglB protein, and then the resultant five sensors showed various affinities that allowed the detection of glucose concentrations ranging from 0.5 μM to 110 mM.[54] The variant $FGBP_{1mM}$ displayed the best performance, with a fluorescence change of ∼600% *in vitro* and a $K_D$ of 1 mM. The fluorescence of $FGBP_{1mM}$ was pH sensitive, and this sensor was used to monitor the glucose transport in *E. coli*. The Green Glifon sensors were developed by inserting the MglB protein into the GFP variant citrine.[55] Three Green Glifon sensors showed an excitation peak at 503 nm and an emission peak at 523 nm, with an ∼450%–600% increase in fluorescence in the presence of glucose and $K_D$ values of 44 μM, 590 μM, and 3.8 mM. All of them responded to glucose and galactose but not to other analogs, and all three exhibited a pH effect. A red version, named Red Glifon, was created by replacing citrine in Green Glifon with the red FP (RFP) mApple and exhibited an excitation maximum of 562 nm and an emission maximum of 591 nm.[56] Two Red Glifon variants bound to glucose with $K_D$ values of 0.3 and 3 mM and showed 330% and 230% dynamic responses, respectively. However, the fluorescence was weak: the brightness of these sensors was ∼1/50 of that of mApple. The Green Glifon and Red Glifon were used to monitor the glucose

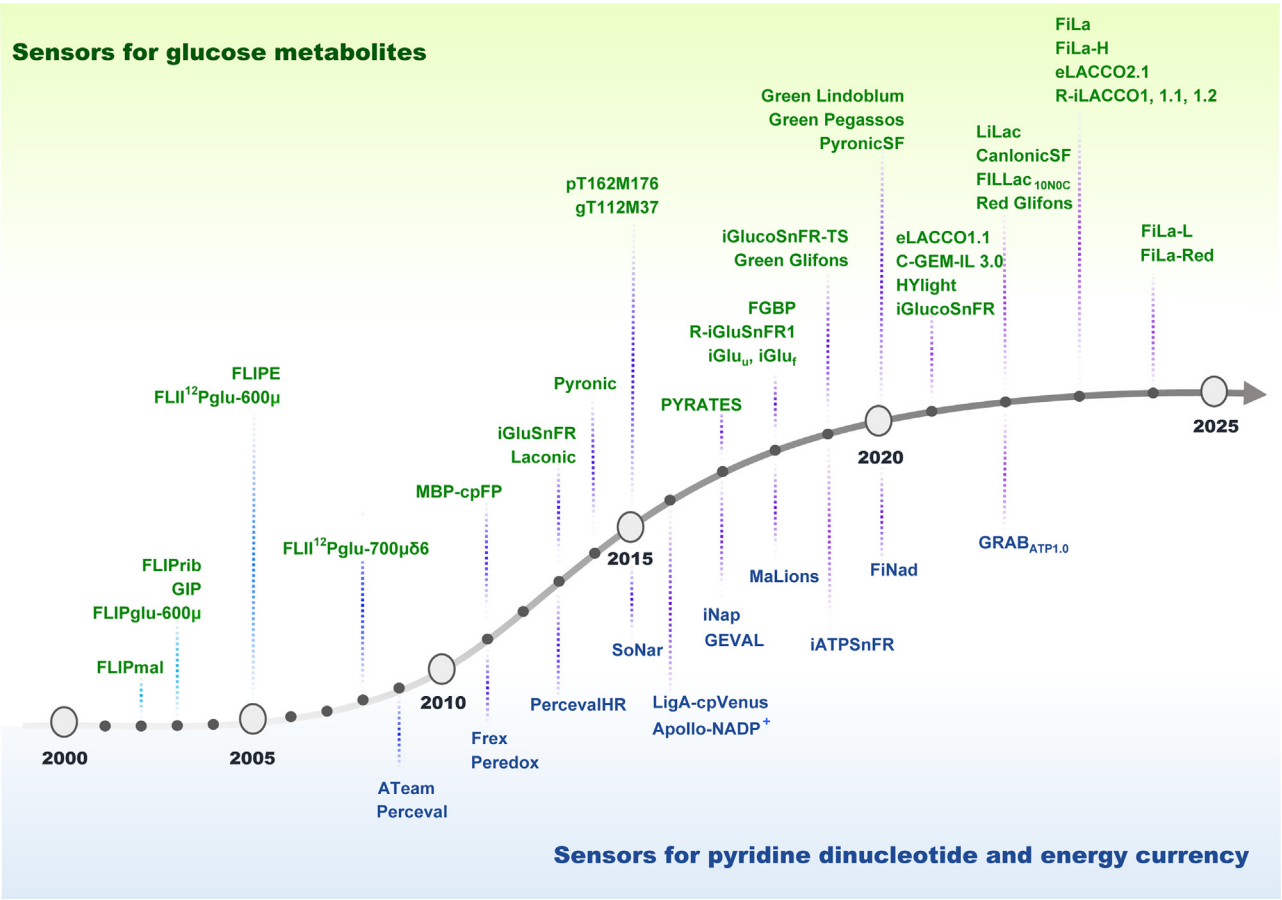


**Figure 3. History of the development of genetically encoded fluorescent sensors for glucose metabolism**

Sensors for glucose metabolites are marked in green and those for pyridine dinucleotide and energy currency in blue.

dynamics in mouse and human cultured cells and in *C. elegans in vivo*. The glucose sensor iGlucoSnFR was developed by inserting cpGFP into the *Thermus thermophilus* GBP.[57] This sensor had one excitation peak at ~485 nm and one emission peak at 515 nm and showed a fluorescence increase of 190% in the presence of glucose with a $K_D$ of 2.3 mM at pH 7.4. Six additional sensors with higher affinity to glucose were created to expand the measurable concentration range. The sensor iGlucoSnFR responded to D-galactose and 2-deoxy-glucose with apparent $K_D$ values of 20 and 45 mM, respectively. The readout of iGlucoSnFR is intensiometric, and the sensor was fused with an RFP to normalize the sensor expression level. This sensor has been applied to monitor glucose levels in *Drosophila*, zebrafish, and mammalian cells.[57] The sensor iGlucoSnFR-TS had a similar design to iGlucoSnFR, but the cpGFP moiety was replaced with the FP T-Sapphire.[58] The resulting sensor had two excitation peaks at ~400 and ~480 nm and one emission peak at 510 nm. At pH values between 7.1 and 7.4, the fluorescence lifetime, as the readout of iGlucoSnFR-TS, increased from ~1.6 to ~1.9 ns as the glucose concentration increased from 0.1 to 10 mM. This sensor was used to measure the glucose concentrations in neurons from acute brain slices and awake mice.

In summary, five FRET-type sensors and five single-FP-type sensors for D-glucose have been established. The previous study shows that five single-FP-type sensors are sensitive to pH. The fluorescence intensities of $FGBP_{1mM}$, Glifons600, Red Glifons, iGlucoSnFR, and iGlucoSnFR-TS elevate by about 25%, 10%–30%, 6%, 3%, and 0.5% with the increase of 0.1 pH units in the apo or substrate-bound state, respectively. It is worth noting that Green Glifon, iGlucoSnFR, and $FGBP_{1mM}$ have been reported to respond to galactose as well as glucose. $FGBP_{1mM}$, Green and Red Glifons, and iGlucoSnFR have comparatively large responses, and their affinities are appropriate for metabolic analysis in living cells considering that typical glucose levels are in the low millimolar range. Therefore, these sensors can be chosen for monitoring glucose in living cells. Fluorescence lifetime is also applicable to the donor species of FRET biosensors. The fluorescence lifetime of FLII$^{12}$Pglu-700μδ6 varies from ~3.3 to ~2.9 ns among single cells[76] and that of iGlucoSnFR-TS varies from ~1.4 to ~1.8 ns in living cells.[58]

### *Sensors for other saccharides*

A series of maltose sensors called FLIPmal were developed by inserting the maltose-binding protein (MBP) into the FRET pair

**Table 1. Fluorescent biosensors for key metabolites of saccharide metabolism**

| Sensor | Sensed metabolite | Sensor origin | FP | Excitation/ emission (∼nm) | $K_D$ (∼μM) or $K_R$ | Dynamic change (∼%) | pH sensitivity (7.0–8.0) |
|---|---|---|---|---|---|---|---|
| Saccharide | | | | | | | |
| FLIPglu-600μ[49] | glucose | *E. coli* MglB | ECFP/EYFP | 430/480, 525 | 590 | 29 | – |
| FLIIP$^{12}$glu-600μ[50] | glucose | *E. coli* MglB | ECFP/EYFP | 430/480, 525 | 600 | 58 | – |
| FLII$^{12}$Pglu-700μδ6[51] | glucose | *E. coli* MglB | ECFP/EYFP | 430/480, 525 | 660 | 74 | – |
| gT112M37[52] | glucose | *E. coli* MglB | ECFP/Venus | 430/480, 530 | 284 | 25 | – |
| GIP[53] | glucose | *E. coli* GBP | $GFP_{UV}$/YFP | 395/510, 527 | 5 | 20 | – |
| $FGBP_{1mM}$[54] | glucose | *E. coli* MglB | cpYFP | 420, 500/515 | 1,000 | 590 | sensitive |
| Green Glifons600[55] | glucose | *E. coli* MglB | citrine | 503/523 | 590 | 400 | sensitive |
| Red Glifons[56] | glucose | *E. coli* MglB | mApple | 562/591 | 320, 3,000 | 330, 230 | sensitive |
| iGlucoSnFR[57] | glucose | *T. thermophilus* GBP | cpGFP | 490/515 | 2,300 | 195 | sensitive |
| iGlucoSnFR-TS[58] | glucose | *T. thermophilus* GBP | cpmTS | 400/510 | 1,000 | 0.3 ns | sensitive |
| FLIPmal[59] | maltose | *E. coli* MBP | ECFP/EYFP | 430/480, 525 | 2.3–226 | 10–20 | – |
| MBP165-cpAzurite, cpCFP, cpGFP, YFP[60] | maltose | *E. coli* MBP | cpAzurite, cpCFP, cpGFP, cpYFP | 383/448, 433/475, 485/515, 515/527 | 2.7, 1,700, 40, 350 | 40, 20, 250 210 | – |
| FLIPrib[61] | ribose | *E. coli* RBP | ECFP/EYFP | 430/480, 525 | 0.25–11,700 | 19–38 | – |
| Glycolytic metabolite | | | | | | | |
| HYlight[62] | FBP | *B. subtilis* CggR | cpGFP | 495, 400/510 | 11, 33[a] | 300 | resistant |
| Pyronic[63] | pyruvate | *E. coli* PdhR | mTFP/Venus | 460/490, 526 | 107 | 24 | – |
| pT162M176[52] | pyruvate | *E. coli* PdhR | ECFP/Venus | 430/480, 530 | 330 | 60 | – |
| PYRATES[64] | pyruvate | *E. coli* PdhR | mTurquoise/ cp173Venus | 430/470, 520 | 65 | 20 | resistant |
| PyronicSF[50] | pyruvate | *E. coli* PdhR | cpGFP | 495/520 | 480 | 250 | sensitive |
| Green Pegassos[65] | pyruvate | *E. coli* PdhR | GFP | 504/516 | 70 | 230 | sensitive |
| Laconic[66] | lactate | *E. coli* LldR | mTFP/Venus | 460/492, 526 | 8, 830 | 8, 11 | sensitive |
| $FILLac_{10N0C}$[67] | lactate | *S. Typhimurium* STLldR | mTFP/Venus | 460/492, 526 | 6.3 | 33 | resistant |
| Green Lindoblum[65] | lactate | *E. coli* LldR | GFP | 500/514 | 30 | 420 | sensitive |
| C-GEM-IL 3.0[68] | lactate | bacterial LldR | sfCFP and sfGFP | 425/490 | 661 | 88 | sensitive |
| CanlonicSF[69] | lactate; $Ca^{2+}$ | *Thermophilus* TTHA0766 | cpGFP | 500/513 | 293 | 190 | sensitive |
| FiLa, FiLa-H, FiLa-L[19,70] | lactate | *E. coli* LldR | cpYFP | 425, 490/514 | 130, 20, 800 | 1,500, 2,600, 700 | sensitive |
| FiLa-Red[71] | lactate | *E. coli* LldR | cpmApple | 570/595 | 460 | 730 | sensitive |
| eLACCO1.1[72] | lactate; $Ca^{2+}$ | *T. thermophilus* TTHA0766 | cpGFP | 398, 493/510 | 3,900 | 400 | sensitive |
| eLACCO2.1[20] | lactate; $Ca^{2+}$ | *T. thermophilus* TTHA0766 | cpGFP | 492/509 | 1,900 | 1,400 | sensitive |
| R-iLACCO1, 1.1, 1.2[20] | lactate | *E. coli* LldR | cpmApple | 574/604 | 74, 230, 350 | 2,000, 2,200, 1,500 | sensitive |
| LiLac[73] | lactate | *H. pylori* TlpC | mTurquoise2 | ∼425/500 | 620, 2,680[b] | 0.8–1.0 ns | resistant |
| Pyridine dinucleotide | | | | | | | |
| Frex[34] | NADH | *B. subtilis* Rex | cpYFP | 421, 500/518 | 3.7, 11[c] | 800 | sensitive[d] |
| LigA-cpVenus[32] | $NAD^+$ | *E. faecalis* LigA | cpVenus | 405, 500/520 | 65 | 100 | sensitive[d] |
| FiNad[33] | $NAD^+$/AXP | *T. aquatics* Rex | cpYFP | ∼500/518 | 1.3[e] | 700 | sensitive[d] |

(*Continued on next page*)

**Table 1. *Continued***

| Sensor | Sensed metabolite | Sensor origin | FP | Excitation/ emission (~nm) | $K_D$ (~μM) or $K_R$ | Dynamic change (~%) | pH sensitivity (7.0–8.0) |
|---|---|---|---|---|---|---|---|
| Peredox[37] | $NAD^+$/NADH | *T. aquatics* Rex | cpT-Sapphire | 400/510 | 330[e] | 150 | resistant |
| SoNar[35] | $NAD^+$/NADH | *T. aquatics* Rex | cpYFP | ~420, 500/518 | 40[e] | 1,500 | sensitive[d] |
| iNap1[39] | NADPH | *T. aquatics* Rex | cpYFP | 420, 500/515 | 2.0 | 900 | sensitive[d] |
| Apollo-$NADP^+$[38] | $NADP^+$ | *H. sapiens* G6PD | FP | tunable spectra | 0.1–20 | 15–20 | resistant |

[a]The apparent $K_D$ of HYlight protein for FBP is 11 μM. In cells, some analogs compete with FBP to bind to the sensor, which shifts the apparent $K_D$ to 33 μM.
[b]At pH 7.3, the apparent $K_D$ values at 24°C and 34°C are 620 and 2,680 μM, respectively.
[c]The apparent $K_D$ values of Frex for NADH were ~3.7 μM at pH 7.4 and ~11 μM at pH 8.0.
[d]Changes in 0.1 pH units would produce about 35%, 25%, 25%, 30%, and 25% changes in fluorescence intensity (or ratio) of Frex, LigA-cpVenus, FiNad, SoNar, and iNap1, respectively.
[e]The apparent $K_R$ (analogous to $K_D$) for the $NAD^+$/AXP ratio or $NAD^+$/NADH ratio at which the response is half-maximal.

ECFP/EYFP.[59] The FLIPmal sensors responded to maltose but not other sugars, showed a 10%–20% dynamic change in the fluorescence ratio, and had three variants with apparent $K_D$ values of ~2.3, ~25, and ~226 μM *in vitro*. These sensors were used for imaging the uptake of maltose in yeast. Marvin et al. developed a small number of single-FP-type maltose sensors by inserting different colors of cpFP (cpAzurite, cpCFP, cpGFP, or cpYFP) into the MBP.[60] The four-colored maltose sensors MBP165-blue, MBP165-cyan, MBP165-green, and MBP165-yellow have affinities with $K_D$ values of ~2.7, ~1,700, ~40, and ~350, respectively, and their fluorescence responses to maltose range from 20% to 250%. These sensors have been used to monitor maltose uptake in *E. coli* and mammalian cells.

A ribose sensor called FLIPrib was constructed by flanking the *E. coli* ribose-binding protein (RBP) with the FRET pair CFP/YFP.[61] FLIPrib-120μ exhibited a 29% fluorescence response in the presence of ribose, with an apparent $K_D$ of ~120 μM. No sugars other than ribose induced a significant response in FLIPrib-120μ. A few variants showed different affinities for ribose, expanding the measurable concentration range by ~5 orders of magnitude. This sensor has been used to report ribose uptake in mammalian cells.

### Sensors for FBP

A fructose-1,6-biphosphate (FBP) sensor named HYlight was developed by inserting cpGFP into the FBP-binding transcriptional repressor CggR from *B. subtilis*.[62] This sensor showed two excitation peaks at ~488 and ~400 nm and one emission peak at ~510 nm. Upon binding to FBP, the fluorescence ratio F488/F400 increased by 300%, with an apparent affinity of 11 μM. However, HYlight could bind fructose-6-phosphate, glucose-6-phosphate, and DHAP, and these competitive ligands gave rise to a shift in the $K_D$ for FBP to 33.0 μM. HYlight also responded to fructose 2,6-bisphosphate with a comparable responsiveness and affinity to FBP. This sensor was used to measure the FBP level in mammalian cells and mouse pancreatic islets.

### Sensors for pyruvate

San Martin et al. engineered a pyruvate sensor named Pyronic by inserting the *E. coli* transcriptional regulator PdhR into the FRET pair mTFP and Venus.[63] Pyronic responded to pyruvate with a dynamic range of ~20% and an apparent $K_D$ of ~107 μM, and the response was resistant to pH perturbation. This sensor showed a slight response to citrate and oxaloacetate. Pyronic was used to report the pyruvate metabolism in single mammalian cells[77,78] and *Drosophila*.[79] In addition, the FRET sensor Pyronic has been characterized for fluorescence lifetime imaging microscopy (FLIM) imaging.[80] The lifetime of the donor species mTFP for Pyronic overlaps with the change in the ratio of intensities between the donor and the acceptor species in cells.[80] Two other FRET-type pyruvate sensors were also built by fusing PdhR with a FRET pair. One sensor created by Peroza et al. had variants with fluorescence ratio changes of 3%–60% and an apparent $K_D$ ranging from 70 to 2,500 μM.[52] These sensors displayed an affinity to lactate more than 100-fold lower than that for pyruvate. The other sensor, mTurquoise-PdhR-cp173Venus, showed a 20% dynamic response and a $K_D$ of 65 μM, and similar to Pyronic, it responded to citrate.[64] Transgenic mice expressing mTurquoise-PdhR-cp173Venus were engineered to analyze the spatiotemporal dynamics of glycolytic activity during mouse embryo mesoderm development. The San Martin group made a modified version of Pyronic, named PyronicSF, which was a single-FP-type sensor designed by the insertion of cpGFP into PdhR.[81] PyronicSF showed two excitation peaks near 488 and 405 nm and one emission peak near 515 nm, and the fluorescence signal excited at 488 nm was used as a typical readout. The sensor showed a 250% dynamic response to pyruvate upon 488 nm excitation, with an apparent $K_D$ of 480 μM. PyronicSF exhibits high selectivity toward pyruvate, with no response to similar metabolites, and the fluorescence response was affected by the pH. The fluorescence intensity excited at 488 nm elevates by about 4%–8% with the increase of 0.1 pH units. The pH effects of PyronicSF may be corrected by the fluorescence excited at the isosbestic point (435 nm) or a parallel measurement of Dead-PyronicSF, a mutated version of PyronicSF almost devoid of pyruvate sensitivity but as sensitive to pH as PyronicSF.[81] This sensor was used to monitor pyruvate metabolism in mouse astrocytes and brain slices of *Drosophila*.[81] Another pyruvate sensor called Green Pegassos has a similar design to PyronicSF, using GFP instead of cpGFP.[65] The sensor had an excitation peak at 504 nm and an emission peak at 516 nm, and it showed a 230% dynamic change in the presence of 1 mM pyruvate with an apparent $K_D$ of 70 μM. This sensor was not affected by organic acids

other than pyruvate, but a pH effect did exist. The fluorescence intensity of Green Pegassos elevates by about 10%–40% with the increase of 0.1 pH units between the apo and substrate-bound states. Green Pegassos was applied to measure the pyruvate level in human induced pluripotent stem cell-derived cardiomyocytes.

### Sensors for lactate

The first genetically encoded lactate sensor was of the FRET type and was designed by fusing the *E. coli* transcription factor LldR with the FRET pair mTFP and Venus.[66] It exhibited two apparent $K_D$ values of ~8 and ~830 μM and a dynamic response of ~10%. In addition, Laconic is also compatible with FLIM imaging.[73] Laconic sensors seem to be partially degraded in mammalian cells.[68] This sensor was used to monitor lactate abundance in blood vessels[82] and pancreatic cells[83] of mice and in *Drosophila*.[79] Another sensor, $FILLac_{10N0C}$, was developed by fusing the LldR homolog from *Salmonella enterica serovar Typhimurium* LT2 with the FRET pair mTFP and Venus.[67] $FILLac_{10N0C}$ exhibited a dynamic fluorescence ratio change of 33% and an apparent $K_D$ of ~6 μM. This sensor responds to neither organic acids other than lactate nor inorganic ions. It was used to measure lactate in bacterial fermentation samples. Recently, increasing effort has been made to develop single-FP-type lactate sensors. The sensor Green Lindoblum, which was designed by fusing GFP with *E. coli* LldR, showed an excitation maximum at 500 nm and an emission maximum at 514 nm.[65] The dynamic response was 420%, and the $K_D$ was 30 μM. Green Lindoblum selectively responded to lactate but not lactate analogs. However, it was reported that puncta appeared when Green Lindoblum was expressed in mammalian cells, and the fluorescence was dim.[20,68] C-GEM-IL 3.0 was a single-FP-type lactate sensor constructed by flanking the bacterial LldR with the split version of the superfolded (sf) proteins sfCFP and sfGFP.[68] The fluorescence spectrum showed one excitation peak at ~425 nm and one emission peak near 490 nm. The sensor selectively responded to lactate, with a dynamic response of ~40%–80% and an apparent $K_D$ of 661 μM. C-GEM-IL 3.0 was further modified to create a pH-resistant sensor variant and a ratiometric variant. Transgenic mouse lines expressing the C-GEM-IL 3.0 construct have been engineered, and lactate dynamics in primary mouse cardiomyocytes have been reported.[68] CanlonicSF was constructed by inserting cpGFP into the *Thermus thermophilus* TTHA0766 protein instead of LldR.[69] This sensor had an excitation peak at ~490 nm and an emission peak at 513 nm, and responded to lactate with a 190% fluorescent change and a $K_D$ of 293 μM. The fluorescence readout was not significantly influenced by lactate analogs, but CanlonicSF depended on calcium to bind to lactate, rendering it sensitive to calcium depletion. This sensor was used to report a lactate pool in the endoplasmic reticulum of mammalian cells, screen inhibitors of the monocarboxylic acid transporter, and track lactate dynamics in fruit flies. Nasu et al. also adopted the TTHA0766 protein for the design of a green lactate sensor, named eLACCO1.1,[72] by the insertion of cpGFP, and a further directed evolution study resulted in the sensor eLACCO2.1 with better performance.[20] eLACCO2.1 exhibited one excitation maximum near 495 nm and one emission maximum near 509 nm. In the presence of lactate, eLACCO2.1 showed a 1,400% increase in fluorescence with an apparent $K_D$ for lactate of 1.9 mM, which represented a significant improvement in responsiveness. eLACCO2.1 was utilized for imaging lactate dynamics in mammalian cells and the mouse brain *in vivo*. As with TTHA0766-based CanlonicSF, the binding of eLACCO1.1 and eLACCO2.1 to lactate was also dependent on $Ca^{2+}$ ion; thus, researchers are concerned with what these sensors actually measure in the complex cellular environment, especially in excitable cells or any cell where $Ca^{2+}$ signaling is expected. Users should be cautious of lactate measurement when deploying these sensors intracellularly.

The FiLa sensor was created by inserting cpYFP into the *E. coli* LldR protein.[19] This sensor had two excitation peaks at ~425 and ~490 nm and an emission peak at 514 nm. Upon binding to lactate, FiLa showed a ~1,500% dynamic change in the fluorescence ratio and an apparent $K_D$ of ~130 μM. A modified version of FiLa, named FiLa-H, exhibited an unprecedented ~2,600% change and higher affinity ($K_D$ of ~20 μM). FiLa displayed stringent selectivity, as it bound only to lactate but no other monocarboxylic acids, dicarboxylic acids, amino acids, ions, or nucleotides. FiLa fluorescence excited at 490 nm was sensitive to pH, whereas the fluorescence excited at 425 nm was relatively pH resistant. This sensor was utilized in the quantification of lactate abundance in organelles of mammalian cells, live mice, and human serum and urine.[19,84,85] A red version of FiLa, named FiLa-Red, was engineered by fusing the cpmApple into the LldR protein.[86] This sensor had an excitation and an emission peak around 570 and 595 nm, respectively. It exhibited a maximal fluorescence change of 730% and an apparent $K_D$ of ~460 μM and was used for multicolor metabolic imaging. Another red fluorescent L-lactate biosensor, named R-iLACCO1, were created by inserting cpmApple into the LldR protein.[20] The sensor exhibited an excitation peak at ~564 nm and an emission peak at ~594 nm. Three variants, R-iLACCO1, R-iLACCO1.1, and R-iLACCO1.2, had up to 2,000%, 2,200%, and 1,500% fluorescent responses to lactate, with $K_D$ values of ~74, ~230, and ~350 μM, respectively. Finally, a lactate sensor with a readout of fluorescence lifetime, called LiLac, was designed by connecting the bacterial chemotaxis protein TlpC from *H. pylori* to mTurquoise2.[73] This sensor selectively responded to lactate but not to other organic acids or calcium. The fluorescence time and affinity of LiLac were dependent on the temperature, with 0.8 ns of dynamic response and an apparent $K_D$ of ~0.62 mM at 24°C but 1 ns and ~2.68 mM at 34°C. Compared to other cpFP-based sensors, LiLac greatly diminished pH sensitivity. In mammalian cells, the lifetime response from LiLac outperforms that of Laconic, displaying a ~6-fold larger response size, reduced variability, and high sensitivity, similar to other high-performance lifetime sensors including Tq-Ca-FLITS and Peredox (~1.3 and ~0.8 ns, respectively).[73]

In summary, seven single-FP-type sensors and two FRET-type sensors for lactate are available. For the pH-sensitive lactate sensor, changes in 0.1 pH units would produce about 1%, 30%–40%, 10%, 2%, 15%, 20%, 10%, 4%–10%, and 0.2%–40% changes in fluorescence intensity (or ratio) of

Laconic, Green Lindoblum, C-GEM-IL 3.0, CanlonicSF, FiLa, FiLa-Red, eLACCO1.1, eLACCO2.1, and R-iLACCO1 in the apo or substrate-bound state, respectively. The green sensor FiLa and the red sensors R-iLACCO1.1 and R-iLACCO1.2 have better performance with regard to specificity, affinity, and responsiveness and thus are recommended for the study of lactate in living cells and *in vivo*. LiLac can be considered if a fluorescence lifetime assay is needed.

### *Guides for application of biosensors*

A few important issues should be considered when using the biosensors to monitor glucose metabolism in living cells. Specificity and responsiveness should be considered first. In addition, the affinity and pH effect of the sensors must be taken into account. The physiological levels of glucose metabolites in mammalian cells vary dramatically. A suitable biosensor should be chosen so as to match its affinity with the physiological level of the metabolite. For the high-abundant metabolites (i.e., glucose, ATP, $NAD^+$, lactate), intracellular levels are typically estimated to be around 0.1–5 mM,[32,87,88] and thus we recommend the low-affinity biosensor for detection of these metabolites. For the low-abundant metabolites (i.e., NADH, $NADP^+$, NADPH), intracellular levels are typically estimated to be around 0.1–30 μM,[34,39,89] and we recommend the high-affinity biosensor. The affinity of each biosensor is listed in Table 1, and some sensors may suffer from limitations due to their inappropriate (physiologically) affinity.

Prokaryotic and eukaryotic cells respond to fluctuations in carbon source availability via regulating the glycolytic rate, and then the accumulation of organic acids may influence pH homeostasis. It has been documented that the intracellular pH fluctuated mildly (pH 6.9–7.0) in bacteria[54,90] when glucose was added to the culture medium; the pH in mammalian cells could be elevated by 0.1–0.4 in response to the manipulation of glucose.[46] Considering that most cpFP-based biosensors are sensitive to the pH fluctuations, it should be a concern that a change in glycolytic rate may alter the intracellular pH and thus interfere with the fluorescence readout of the sensors. In many circumstances, the effects of pH on cpFP-based sensors are not evident.[19,39,91] However, when intracellular pH fluctuations do occur, the pH effects should be corrected for quantitative measurements by the pH-control sensor. Take the lactate sensor FiLa as an example: FiLa and FiLa-C have similar pH responses; however, only FiLa responds to lactate fluctuations. For quantitative measurements, the pH effects on FiLa fluorescence were corrected by expressing FiLa and FiLa-C separately in the cells and measuring the fluorescence of these cells in parallel. The lactate level was calculated according to the pH-corrected ratio (*R*) of the FiLa sensor, i.e., $R_{FiLa}/R_{FiLa\text{-}C}$, which is largely pH insensitive.[19] Similar approaches were used successfully for quantitative measurement of other metabolites, such as NADH, NADH/$NAD^+$, NADPH, and $NAD^+$, using genetically encoded sensors.[32,34,39,91,92] It should be noted that the FiLa and FiLa-C signals could not be deconvolved in the same cells because of similar fluorescence emission spectra. To simultaneously image lactate and pH in single living cells, users can generate a dual-function, genetically encoded sensor by fusing the FiLa sensor and the pH-sensitive RFP.[93]

## ILLUSTRATING GLUCOSE METABOLISM WITH SENSORS

### Visualizing local and compartmentalized metabolism of glycolytic intermediates

A few studies have offered novel insights into glucose metabolism at subcellular resolution by using biosensors. It is not yet fully understood how cellular mobility, an energy-demanding process, is coupled with glycolysis, the primary energy-generating mechanism in the cytoplasm. By using the lactate sensor Laconic and deep-learning-enabled image analysis, Wu et al. showed that the small GTPase RhoA coordinated stress-fiber formation and the translocation of glucose transporters onto the plasma membrane.[94] Sites with a high lactate production rate were colocalized with cytoskeletal remodeling areas within single endothelial cells. Another example is involved in the local production of acetyl-CoA from pyruvate at DNA damage foci. Double-strand breaks in DNA will trigger the DNA damage response, with histone-acetylation-mediated chromatin relaxation preceding DNA repair. Recently, Zhang et al. reported that the nuclear pyruvate dehydrogenase isoform PDHE1α was recruited to DNA damage loci.[95] By using the pyruvate sensor PyronicSF, they showed that the local production of acetyl-CoA by PDHE1α facilitated chromatin remodeling and, thus, DNA repair.

Moreover, lactate has been proposed to be directly imported into mitochondria for energy production, but definitive, consistent evidence supporting this hypothesis is lacking, which has resulted in a long-standing debate. Li et al. utilized the mitochondrial-targeted lactate sensor FiLa to show that lactate was enriched in mitochondria, and the super-resolution imaging suggested that lactate was localized in the matrix but not in the membrane or the intermembrane space.[19] A biochemical assay for lactate resulted in a similar observation. By simultaneously imaging cytosolic and mitochondrial lactate with iLACCO1 and R-iLACCO1.2, respectively, Nasu et al. observed lactate with a concomitant increase in the cytosol and mitochondria when glucose was fed, implying that lactate produced in the cytosol is also shuttled to the mitochondrial matrix.[20] Furthermore, Cai et al. reported that mitochondrial lactate could not be directly converted into pyruvate but could activate the mitochondrial electron transport chain and thus enhance energy production.[96]

### Monitoring heterogeneous glucose metabolites at single-cell resolution

Biosensor-based assays allow the monitoring of glucose metabolites at single-cell resolution and have revealed widespread intercellular metabolic heterogeneity. By using the glucose sensor FLII12Pglu-700μδ6, Wollman studied the response of glucose uptake by adipocytes to insulin.[97] Metabolic imaging showed that the body size of adipocytes affected glucose uptake and utilization, with larger adipocytes being less sensitive to insulin than smaller adipocytes. One of the most studied cases is in cancer cells. Kondo exploited the FLII12Pglu-700μδ6 and AT1.03 sensors to demonstrate that breast cancer cells exhibited a considerable heterogeneity in glucose metabolism, even for cells expanded from a single-cell clone, indicating a nongenetic but metabolic source of heterogeneity.[76] The cell

population with high intracellular glucose levels had low mitochondrial membrane potential and low levels of radical oxygen species. Interestingly, time-resolved tracking showed that the glycolytic state was heritable through mitosis. This glucose abundance was regulated by PI3K signaling, bromodomain function, and cofilin activity. The heterogeneity of glucose metabolism in tumor cells exerts an important effect on the development and progression of tumors. By utilizing the NADH/$NAD^+$ sensor SoNar to analyze energy metabolism in leukemic cells, Hao et al. found that leukemic cells of the $SoNar^{high}$ subpopulation (high NADH/$NAD^+$ level) proliferated rapidly, tended to cleave symmetrically, and possessed potent leukemogenic ability compared to their $SoNar^{low}$ counterparts.[98]

### Real-time monitoring of glucose metabolism in live animals

A few *in vivo* studies using biosensors have offered unique insights into glucose metabolism, and here we take some intriguing findings in neuroscience as examples. It is an important question which fuel supports energy-demanding neuronal activities. A hypothesis, named astrocyte-neuron lactate shuttle, proposes that astrocytes vigorously consume glucose and release lactate, which is used by the neighboring neurons as a crucial fuel. In a study, the lactate sensor Laconic was expressed in astrocytes and neurons in mouse brains with lineage-specific promoters.[99] Under the anesthesia condition, intravenous injection of lactate induced a larger increase of Laconic signals in neurons than astrocytes, whereas injection of pyruvate decreased the fluorescent signals more in astrocytes than neurons, implicating a gradient of lactate abundance from astrocytes to neurons in brain at rest. Another study using the NADH/$NAD^+$ sensor Peredox reports that glucose is actively utilized by neurons during activation.[100] Fluorescence lifetime imaging of the Peredox sensor showed, with single-cell resolution, that NADH/$NAD^+$ transiently rose for 4–5 min in layer 2/3 neurons in the whisker-sensing region of primary somatosensory cortex of awake mice after a 10 s whisker stimulation was applied, while the neighboring non-responsive neurons showed no significant change. This NADH/$NAD^+$ elevation could not be diminished by manipulating the monocarboxylate transporter inhibitor, indicating that glucose, rather than lactate, metabolism likely has a critically supportive role in neuronal activity.[100] Moreover, a recent study used the invariant developmental lineage of *C. elegans* and demonstrated that their different types of neurons seemed to have an intrinsic glycolytic capacity.[101] Metabolic imaging using the FBP sensor HYlight showed that three neurons located in worm tails had a significantly different abundance of FBP and that the metabolic patterns were invariant across individual worms. All of these observations exhibit the unparalleled spatiotemporal resolution of biosensor assays in living organisms as compared to conventional metabolic analysis technologies.

## CONCLUSIONS AND FUTURE PERSPECTIVES

The past few years have seen the rapid development of biosensor-based metabolite monitoring technology. This powerful tool effectively complements omics technologies, such as transcriptomic profiling based on single-cell RNA sequencing technology and metabolomics profiling based on mass spectrometry and nuclear magnetic resonance spectrometry. While omics analysis compiles globally molecular features, biosensor-based metabolic monitoring can track the spatial distribution and temporal fluctuation of small-molecule metabolites in living cells and *in vivo* in real time. As glucose metabolites function as energy carriers, building blocks of biomass, indicators of redox status, and messengers of biochemical information, they have been intensively studied. Nevertheless, high-quality biosensors remain lacking for many key glucose metabolites, such as glucose-6-phosphate, the starting metabolite for both glycolysis and PPP; DHAP, which links glucose and glycerol metabolism; glycerate-3-phosphate, which connects glucose with serine and glycine metabolism; PEP, a common metabolite on the glycolysis and gluconeogenesis pathways; ribose-5-phosphate, which connects the PPP with nucleotide metabolism; and fructose, mannose, and other saccharides. For a high-quality sensor, stringent selectivity, high responsiveness, and appropriate affinity are crucial requirements. In addition, bright fluorescence intensity, a ratiometric readout, rapid binding/dissociation dynamics, and robust resistance to pH and temperature changes are highly favorable.

It is a great challenge to develop a high-quality biosensor that can fulfill all the above criteria. A typical approach for biosensor development is to combine the structure-guided design strategy with a high-throughput screening of mutant libraries.[19,20] This approach is labor intensive, and some automatic high-throughput screening platforms have been innovated recently. Faculae is a microscope imaging-guided cell selection strategy that evaluates tens of thousands of variants in cultured mammalian cells at one time.[102] In faculae screening, mammalian cells with genomic integration of biosensor libraries are focally illuminated at single-cell resolution, and then candidate cells are retrieved through fluorescence-activated cell sorting, followed by genotyping. Compared to the screening of faculae in living cells, a platform named BeadScan utilizes droplet microfluidics to screen libraries of *in-vitro*-translated sensors.[73] In the BeadScan system, a DNA library is made in water-in-oil droplets to allow the amplification of ~2 kb sensor-coding sequences; the emulsion PCR droplets are then fused with an *in vitro* transcription/translation system to ensure an efficient synthesis of sensor proteins; finally, each sensor variant is trapped in a semipermeable gel, which enables the exchange of analytes and ions. By recording the fluorescent intensity or lifetime, this system can evaluate specificity, responsiveness, pH sensitivity, and affinity under various conditions. The other way is to leverage artificial intelligence technology to promote high-quality sensor development. Classic machine learning methods[103] and deep learning models[104] have been used to accelerate the directed evolution of biosensor engineering. Moreover, explainable learning models are promising for finding a general strategy to govern the development of high-quality sensors, for example, to identify metabolites with biochemical and structural similarities such as different forms of monosaccharides and monocarboxylic acids.

Generally, the level of biosensors expressed in the cells may be around 1–10 μM, depending on cell types, gene-transfer efficiency, promoters, and other factors. For the high-abundant

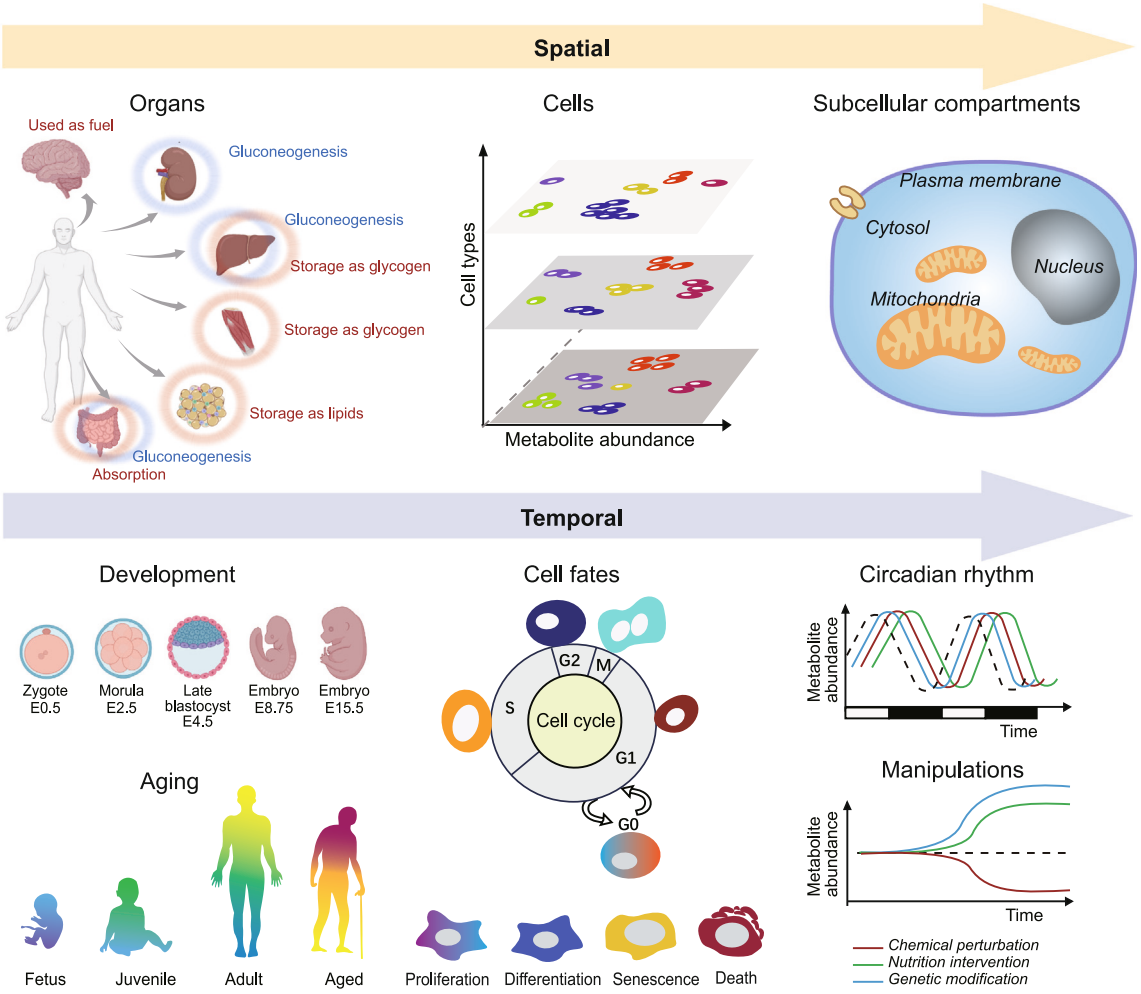


**Figure 4. Analysis of the spatiotemporal dynamics of glucose metabolites by genetically encoded biosensors**

Biosensors are powerful tools for monitoring the glucose metabolites at multiple spatial and temporal scales, and a few typical scenarios for application of biosensors are presented here. Sensors can be used to detect the metabolite levels in organs that are critical for glucose absorption, production, storage, and utilization (top left), at single-cell resolution such that they differentiate metabolically heterogeneous populations (top middle), and at subcellular resolution to offer insight into the transport and local metabolism of glucose metabolites (top right). Time-resolved metabolic imaging with biosensors can be exploited for tracking the glucose metabolism in durable processes such as embryonic development (bottom left), in biological processes with shorter timescales such as cell cycle progression and cell fate decision (bottom middle), and in circadian rhythm and metabolic responses to manipulations such as chemical perturbation, nutrient intervention, and genetic modifications (bottom right).

metabolites in glucose metabolism, intracellular levels are estimated to be in the millimolar range, which is much higher than the sensor's level; however, for the low-abundant metabolites, i.e., NADH and $NADP^+$, their free levels are around 0.1–0.2 μM[34,89] in the cytosol, which is much lower than the sensor's level. It is reasonable to raise the concern that too much sensing of low-abundant metabolites in the cells, but not the sensing of high-abundant metabolites, may contribute to the temporal buffering effect, similar to the observation in the $Ca^{2+}$ sensor GCaMP.[105] It is interesting that we did not observe a significant "buffering or depleting" effect of high-affinity NADH or NADPH sensors such as SoNar or iNap1, which responds immediately to exogenous pyruvate, lactate, glucose, or oxidants,[39,91] suggesting there were minimal temporal buffering effects. In addition, we did not notice any significant perturbation of the cellular metabolic state, cell growth, or developmental efficiency *in vitro* or the birth ratio *in vivo* of mouse embryos by high expression of the sensor itself.[106] One explanation is that there are already buffering systems for NADH and NADPH in the cells, which consist of many NADH- or NADPH-binding proteins in the cells. However, for other low-abundant metabolites, caution should is warranted to avoid the potential buffering effect of overexpressed biosensors.

Biosensors can be used to conveniently monitor the spatial distribution and dynamic fluctuation of glucose metabolites at multiple scales (Figure 4). On one side, by transgenic technology or other gene delivery and expression systems, biosensors are capable of detecting the metabolite levels in organs for glucose

absorption and production (intestine, liver, and kidney), storage (liver and muscle), and utilization with glucose as an obligatory energy source (e.g., brain and red blood cells). By performing metabolic monitoring at single-cell resolution, sensors can quantitatively report the cellular heterogeneity in glucose metabolism and the diversity derived from either the intrinsically metabolic program of cells or the cellular position in the nutrient microenvironment (Figure 4). An increasing amount of data reveal that this process is important under various physiological and pathological conditions. Furthermore, sensors can visualize the glucose metabolite abundance in specific organelles, membraneless granules, and smaller spaces. On the other hand, biosensors enable either durable or transient monitoring of glucose metabolites in living cells and *in vivo* (Figure 4). For example, long-term tracking can be performed during the embryonic development and aging processes. Moreover, sensors can be exploited as quantitative metabolic reporters in various cellular and physiological processes during which glucose metabolites have relatively rapid fluctuation, such as cell cycle progression, differentiation, cell death, circadian rhythm, feeding and fasting, physical and brain activity, immune response, and stress. Time-resolving imaging can record the transient modulation of glucose metabolism such as that linked to cytoskeletal remodeling. In addition to physiological dynamics, sensors are useful for monitoring the responses of glucose metabolism to nutritional, chemical, and genetic manipulation in mechanistic study and drug development. With the increasing development and application of metabolite biosensors, data processing methods enabled by computer vision have been developed for the analysis of metabolic imaging data. The software package FRETzel permits automatic cell segmentation and glucose quantitation using the glucose sensor-based imaging data,[97] and a deep-learning-enabled image analysis of lactate sensor data can calculate the lactate production rate in endothelial cells at the single-cell level.[107] These highly efficient tools for sensor engineering and data processing could be invaluable for understanding glucose metabolism in health and disease.

## ACKNOWLEDGMENTS

We apologize that some works on glucose metabolism and the related sensors are not cited due to space constraints. This research is supported by the National Key Research and Development Program of China (2019YFA0904800 and 2023YFA1802000), NSFC (32030065, 32150030, 32394001, 32121005, 92049304, and 32471361), the Natural Science Foundation of Shanghai (23ZR1415800), the Shanghai Frontiers Science Center of Optogenetic Techniques for Cell Metabolism, the Research Unit of New Techniques for Live-cell Metabolic Imaging (Chinese Academy of Medical Sciences, 2019-I2M-5-013), the State Key Laboratory of Bioreactor Engineering, and the Fundamental Research Funds for the Central Universities.

## DECLARATION OF INTERESTS

The authors declare no competing interests.

## REFERENCES

1. Schjoldager, K.T., Narimatsu, Y., Joshi, H.J., and Clausen, H. (2020). Global view of human protein glycosylation pathways and functions. Nat. Rev. Mol. Cell Biol. *21*, 729–749. https://doi.org/10.1038/s41580-020-00294-x.
2. Li, X., Gianoulis, T.A., Yip, K.Y., Gerstein, M., and Snyder, M. (2010). Extensive in vivo metabolite-protein interactions revealed by large-scale systematic analyses. Cell *143*, 639–650. https://doi.org/10.1016/j.cell.2010.09.048.
3. Piazza, I., Kochanowski, K., Cappelletti, V., Fuhrer, T., Noor, E., Sauer, U., and Picotti, P. (2018). A Map of Protein-Metabolite Interactions Reveals Principles of Chemical Communication. Cell *172*, 358–372.e23. https://doi.org/10.1016/j.cell.2017.12.006.
4. Liu, W., Wang, Y., Bozi, L.H.M., Fischer, P.D., Jedrychowski, M.P., Xiao, H., Wu, T., Darabedian, N., He, X., Mills, E.L., et al. (2023). Lactate regulates cell cycle by remodelling the anaphase promoting complex. Nature *616*, 790–797. https://doi.org/10.1038/s41586-023-05939-3.
5. Zhang, W., Wang, G., Xu, Z.G., Tu, H., Hu, F., Dai, J., Chang, Y., Chen, Y., Lu, Y., Zeng, H., et al. (2019). Lactate is a natural suppressor of RLR signaling by targeting MAVS. Cell *178*, 176–189.e15. https://doi.org/10.1016/j.cell.2019.05.003.
6. Wan, N., Wang, N., Yu, S., Zhang, H., Tang, S., Wang, D., Lu, W., Li, H., Delafield, D.G., Kong, Y., et al. (2022). Cyclic immonium ion of lactyllysine reveals widespread lactylation in the human proteome. Nat. Methods *19*, 854–864. https://doi.org/10.1038/s41592-022-01523-1.
7. Zhang, D., Tang, Z., Huang, H., Zhou, G., Cui, C., Weng, Y., Liu, W., Kim, S., Lee, S., Perez-Neut, M., et al. (2019). Metabolic regulation of gene expression by histone lactylation. Nature *574*, 575–580. https://doi.org/10.1038/s41586-019-1678-1.
8. Chen, Y., Wu, J., Zhai, L., Zhang, T., Yin, H., Gao, H., Zhao, F., Wang, Z., Yang, X., Jin, M., et al. (2024). Metabolic regulation of homologous recombination repair by MRE11 lactylation. Cell *187*, 294–311.e21. https://doi.org/10.1016/j.cell.2023.11.022.
9. Orozco, J.M., Krawczyk, P.A., Scaria, S.M., Cangelosi, A.L., Chan, S.H., Kunchok, T., Lewis, C.A., and Sabatini, D.M. (2020). Dihydroxyacetone phosphate signals glucose availability to mTORC1. Nat. Metab. *2*, 893–901. https://doi.org/10.1038/s42255-020-0250-5.
10. Zhang, J.J., Fan, T.T., Mao, Y.Z., Hou, J.L., Wang, M., Zhang, M., Lin, Y., Zhang, L., Yan, G.Q., An, Y.P., et al. (2021). Nuclear dihydroxyacetone phosphate signals nutrient sufficiency and cell cycle phase to global histone acetylation. Nat. Metab. *3*, 859–875. https://doi.org/10.1038/s42255-021-00405-8.
11. Wang, C., Huang, M., Lin, Y., Zhang, Y., Pan, J., Jiang, C., Cheng, M., Li, S., He, W., Li, Z., et al. (2023). ENO2-derived phosphoenolpyruvate functions as an endogenous inhibitor of HDAC1 and confers resistance to antiangiogenic therapy. Nat. Metab. *5*, 1765–1786. https://doi.org/10.1038/s42255-023-00883-y.
12. Boukouris, A.E., Zervopoulos, S.D., and Michelakis, E.D. (2016). Metabolic Enzymes Moonlighting in the Nucleus: Metabolic Regulation of Gene Transcription. Trends Biochem. Sci. *41*, 712–730. https://doi.org/10.1016/j.tibs.2016.05.013.
13. Pantaleon, M., Ryan, J.P., Gil, M., and Kaye, P.L. (2001). An unusual subcellular localization of GLUT1 and link with metabolism in oocytes and preimplantation mouse embryos. Biol. Reprod. *64*, 1247–1254. https://doi.org/10.1095/biolreprod64.4.1247.
14. Sutendra, G., Kinnaird, A., Dromparis, P., Paulin, R., Stenson, T.H., Haromy, A., Hashimoto, K., Zhang, N., Flaim, E., and Michelakis, E.D. (2014). A nuclear pyruvate dehydrogenase complex is important for the generation of acetyl-CoA and histone acetylation. Cell *158*, 84–97. https://doi.org/10.1016/j.cell.2014.04.046.
15. Nagaraj, R., Sharpley, M.S., Chi, F., Braas, D., Zhou, Y., Kim, R., Clark, A.T., and Banerjee, U. (2017). Nuclear Localization of Mitochondrial TCA Cycle Enzymes as a Critical Step in Mammalian Zygotic Genome Activation. Cell *168*, 210–223.e11. https://doi.org/10.1016/j.cell.2016.12.026.
16. Dasovich, M., and Leung, A.K.L. (2023). PARPs and ADP-ribosylation: Deciphering the complexity with molecular tools. Mol. Cell *83*, 1552–1572. https://doi.org/10.1016/j.molcel.2023.04.009.

17. Wolfram-Schauerte, M., and Höfer, K. (2023). NAD-capped RNAs - a redox cofactor meets RNA. Trends Biochem. Sci. *48*, 142–155. https://doi.org/10.1016/j.tibs.2022.08.004.

18. Ryu, K.W., Nandu, T., Kim, J., Challa, S., DeBerardinis, R.J., and Kraus, W.L. (2018). Metabolic regulation of transcription through compartmentalized NAD(+) biosynthesis. Science *360*, eaan5780. https://doi.org/10.1126/science.aan5780.

19. Li, X., Zhang, Y., Xu, L., Wang, A., Zou, Y., Li, T., Huang, L., Chen, W., Liu, S., Jiang, K., et al. (2023). Ultrasensitive sensors reveal the spatiotemporal landscape of lactate metabolism in physiology and disease. Cell Metab. *35*, 200–211.e9. https://doi.org/10.1016/j.cmet.2022.10.002.

20. Nasu, Y., Aggarwal, A., Le, G.N.T., Vo, C.T., Kambe, Y., Wang, X., Beinlich, F.R.M., Lee, A.B., Ram, T.R., Wang, F., et al. (2023). Lactate biosensors for spectrally and spatially multiplexed fluorescence imaging. Nat. Commun. *14*, 6598. https://doi.org/10.1038/s41467-023-42230-5.

21. Diaz-Ruiz, R., Averet, N., Araiza, D., Pinson, B., Uribe-Carvajal, S., Devin, A., and Rigoulet, M. (2008). Mitochondrial oxidative phosphorylation is regulated by fructose 1,6-bisphosphate. A possible role in Crabtree effect induction? J. Biol. Chem. *283*, 26948–26955. https://doi.org/10.1074/jbc.M800408200.

22. Rosas Lemus, M., Roussarie, E., Hammad, N., Mougeolle, A., Ransac, S., Issa, R., Mazat, J.P., Uribe-Carvajal, S., Rigoulet, M., and Devin, A. (2018). The role of glycolysis-derived hexose phosphates in the induction of the Crabtree effect. J. Biol. Chem. *293*, 12843–12854. https://doi.org/10.1074/jbc.RA118.003672.

23. De Jesus, A., Keyhani-Nejad, F., Pusec, C.M., Goodman, L., Geier, J.A., Stoolman, J.S., Stanczyk, P.J., Nguyen, T., Xu, K., Suresh, K.V., et al. (2022). Hexokinase 1 cellular localization regulates the metabolic fate of glucose. Mol. Cell *82*, 1261–1277.e9. https://doi.org/10.1016/j.molcel.2022.02.028.

24. Kohnhorst, C.L., Kyoung, M., Jeon, M., Schmitt, D.L., Kennedy, E.L., Ramirez, J., Bracey, S.M., Luu, B.T., Russell, S.J., and An, S. (2017). Identification of a multienzyme complex for glucose metabolism in living cells. J. Biol. Chem. *292*, 9191–9203. https://doi.org/10.1074/jbc.M117.783050.

25. Jeon, M., Chauhan, K.M., Szeto, G.L., Kyoung, M., and An, S. (2022). Subcellular regulation of glucose metabolism through multienzyme glucosome assemblies by EGF-ERK1/2 signaling pathways. J. Biol. Chem. *298*, 101675. https://doi.org/10.1016/j.jbc.2022.101675.

26. Fuller, G.G., and Kim, J.K. (2021). Compartmentalization and metabolic regulation of glycolysis. J. Cell Sci. *134*, jcs258469. https://doi.org/10.1242/jcs.258469.

27. Jang, S., Nelson, J.C., Bend, E.G., Rodríguez-Laureano, L., Tueros, F.G., Cartagenova, L., Underwood, K., Jorgensen, E.M., and Colón-Ramos, D.A. (2016). Glycolytic Enzymes Localize to Synapses under Energy Stress to Support Synaptic Function. Neuron *90*, 278–291. https://doi.org/10.1016/j.neuron.2016.03.011.

28. Salvi, A.M., Bays, J.L., Mackin, S.R., Mege, R.M., and DeMali, K.A. (2021). Ankyrin G organizes membrane components to promote coupling of cell mechanics and glucose uptake. Nat. Cell Biol. *23*, 457–466. https://doi.org/10.1038/s41556-021-00677-y.

29. De Bock, K., Georgiadou, M., Schoors, S., Kuchnio, A., Wong, B.W., Cantelmo, A.R., Quaegebeur, A., Ghesquière, B., Cauwenberghs, S., Eelen, G., et al. (2013). Role of PFKFB3-driven glycolysis in vessel sprouting. Cell *154*, 651–663. https://doi.org/10.1016/j.cell.2013.06.037.

30. Hu, H., Juvekar, A., Lyssiotis, C.A., Lien, E.C., Albeck, J.G., Oh, D., Varma, G., Hung, Y.P., Ullas, S., Lauring, J., et al. (2016). Phosphoinositide 3-Kinase Regulates Glycolysis through Mobilization of Aldolase from the Actin Cytoskeleton. Cell *164*, 433–446. https://doi.org/10.1016/j.cell.2015.12.042.

31. Qian, Y., Rancic, V., Wu, J., Ballanyi, K., and Campbell, R.E. (2019). A Bioluminescent Ca(2+) Indicator Based on a Topological Variant of GCaMP6s. Chembiochem *20*, 516–520. https://doi.org/10.1002/cbic.201800255.

32. Cambronne, X.A., Stewart, M.L., Kim, D., Jones-Brunette, A.M., Morgan, R.K., Farrens, D.L., Cohen, M.S., and Goodman, R.H. (2016). Biosensor reveals multiple sources for mitochondrial NAD(+). Science *352*, 1474–1477. https://doi.org/10.1126/science.aad5168.

33. Zou, Y., Wang, A., Huang, L., Zhu, X., Hu, Q., Zhang, Y., Chen, X., Li, F., Wang, Q., Wang, H., et al. (2020). Illuminating $NAD^+$ Metabolism in Live Cells and In Vivo Using a Genetically Encoded Fluorescent Sensor. Dev. Cell *53*, 240–252.e7. https://doi.org/10.1016/j.devcel.2020.02.017.

34. Zhao, Y., Jin, J., Hu, Q., Zhou, H.M., Yi, J., Yu, Z., Xu, L., Wang, X., Yang, Y., and Loscalzo, J. (2011). Genetically encoded fluorescent sensors for intracellular NADH detection. Cell Metab. *14*, 555–566. https://doi.org/10.1016/j.cmet.2011.09.004.

35. Zhao, Y., Hu, Q., Cheng, F., Su, N., Wang, A., Zou, Y., Hu, H., Chen, X., Zhou, H.M., Huang, X., et al. (2015). SoNar, a Highly Responsive NAD+/NADH Sensor, Allows High-Throughput Metabolic Screening of Anti-tumor Agents. Cell Metab. *21*, 777–789. https://doi.org/10.1016/j.cmet.2015.04.009.

36. Zhao, Y., Wang, A., Zou, Y., Su, N., Loscalzo, J., and Yang, Y. (2016). In vivo monitoring of cellular energy metabolism using SoNar, a highly responsive sensor for NAD(+)/NADH redox state. Nat. Protoc. *11*, 1345–1359. https://doi.org/10.1038/nprot.2016.074.

37. Hung, Y.P., Albeck, J.G., Tantama, M., and Yellen, G. (2011). Imaging cytosolic NADH-NAD(+) redox state with a genetically encoded fluorescent biosensor. Cell Metab. *14*, 545–554. https://doi.org/10.1016/j.cmet.2011.08.012.

38. Cameron, W.D., Bui, C.V., Hutchinson, A., Loppnau, P., Gräslund, S., and Rocheleau, J.V. (2016). Apollo-NADP(+): a spectrally tunable family of genetically encoded sensors for NADP(+). Nat. Methods *13*, 352–358. https://doi.org/10.1038/nmeth.3764.

39. Tao, R., Zhao, Y., Chu, H., Wang, A., Zhu, J., Chen, X., Zou, Y., Shi, M., Liu, R., Su, N., et al. (2017). Genetically encoded fluorescent sensors reveal dynamic regulation of NADPH metabolism. Nat. Methods *14*, 720–728. https://doi.org/10.1038/nmeth.4306.

40. Zou, Y., Wang, A., Shi, M., Chen, X., Liu, R., Li, T., Zhang, C., Zhang, Z., Zhu, L., Ju, Z., et al. (2018). Analysis of redox landscapes and dynamics in living cells and in vivo using genetically encoded fluorescent sensors. Nat. Protoc. *13*, 2362–2386. https://doi.org/10.1038/s41596-018-0042-5.

41. Imamura, H., Nhat, K.P.H., Togawa, H., Saito, K., Iino, R., Kato-Yamada, Y., Nagai, T., and Noji, H. (2009). Visualization of ATP levels inside single living cells with fluorescence resonance energy transfer-based genetically encoded indicators. Proc. Natl. Acad. Sci. USA *106*, 15651–15656. https://doi.org/10.1073/pnas.0904764106.

42. Tsuyama, T., Kishikawa, J.i., Han, Y.W., Harada, Y., Tsubouchi, A., Noji, H., Kakizuka, A., Yokoyama, K., Uemura, T., and Imamura, H. (2013). In vivo fluorescent adenosine 5'-triphosphate (ATP) imaging of Drosophila melanogaster and Caenorhabditis elegans by using a genetically encoded fluorescent ATP biosensor optimized for low temperatures. Anal. Chem. *85*, 7889–7896. https://doi.org/10.1021/ac4015325.

43. Lobas, M.A., Tao, R., Nagai, J., Kronschläger, M.T., Borden, P.M., Marvin, J.S., Looger, L.L., and Khakh, B.S. (2019). A genetically encoded single-wavelength sensor for imaging cytosolic and cell surface ATP. Nat. Commun. *10*, 711. https://doi.org/10.1038/s41467-019-08441-5.

44. Wu, Z., He, K., Chen, Y., Li, H., Pan, S., Li, B., Liu, T., Xi, F., Deng, F., Wang, H., et al. (2022). A sensitive GRAB sensor for detecting extracellular ATP in vitro and in vivo. Neuron *110*, 770–782.e5. https://doi.org/10.1016/j.neuron.2021.11.027.

45. Arai, S., Kriszt, R., Harada, K., Looi, L.S., Matsuda, S., Wongso, D., Suo, S., Ishiura, S., Tseng, Y.H., Raghunath, M., et al. (2018). RGB-Color Intensiometric Indicators to Visualize Spatiotemporal Dynamics of ATP in Single Cells. Angew. Chem. Int. Ed. Engl. *57*, 10873–10878. https://doi.org/10.1002/anie.201804304.

46. Berg, J., Hung, Y.P., and Yellen, G. (2009). A genetically encoded fluorescent reporter of ATP:ADP ratio. Nat. Methods *6*, 161–166. https://doi.org/10.1038/nmeth.1288.

47. Tantama, M., Martínez-François, J.R., Mongeon, R., and Yellen, G. (2013). Imaging energy status in live cells with a fluorescent biosensor of the intracellular ATP-to-ADP ratio. Nat. Commun. *4*, 2550. https://doi.org/10.1038/ncomms3550.

48. Zhang, Z., Cheng, X., Zhao, Y., and Yang, Y. (2020). Lighting Up Live-Cell and In Vivo Central Carbon Metabolism with Genetically Encoded Fluorescent Sensors. Annu. Rev. Anal. Chem. *13*, 293–314. https://doi.org/10.1146/annurev-anchem-091619-091306.

49. Fehr, M., Lalonde, S., Lager, I., Wolff, M.W., and Frommer, W.B. (2003). In vivo imaging of the dynamics of glucose uptake in the cytosol of COS-7 cells by fluorescent nanosensors. J. Biol. Chem. *278*, 19127–19133, [pii]. https://doi.org/10.1074/jbc.M301333200.

50. Deuschle, K., Okumoto, S., Fehr, M., Looger, L.L., Kozhukh, L., and Frommer, W.B. (2005). Construction and optimization of a family of genetically encoded metabolite sensors by semirational protein engineering. Protein Sci. *14*, 2304–2314. https://doi.org/10.1110/ps.051508105.

51. Takanaga, H., Chaudhuri, B., and Frommer, W.B. (2008). GLUT1 and GLUT9 as major contributors to glucose influx in HepG2 cells identified by a high sensitivity intramolecular FRET glucose sensor. Biochim. Biophys. Acta *1778*, 1091–1099. https://doi.org/10.1016/j.bbamem.2007.11.015.

52. Peroza, E.A., Boumezbeur, A.H., and Zamboni, N. (2015). Rapid, randomized development of genetically encoded FRET sensors for small molecules. Analyst *140*, 4540–4548. https://doi.org/10.1039/c5an00707k.

53. Ye, K., and Schultz, J.S. (2003). Genetic engineering of an allosterically based glucose indicator protein for continuous glucose monitoring by fluorescence resonance energy transfer. Anal. Chem. *75*, 3451–3459. https://doi.org/10.1021/ac034022q.

54. Hu, H., Wei, Y., Wang, D., Su, N., Chen, X., Zhao, Y., Liu, G., and Yang, Y. (2018). Glucose monitoring in living cells with single fluorescent protein-based sensors. RSC Adv. *8*, 2485–2489. https://doi.org/10.1039/c7ra11347a.

55. Mita, M., Ito, M., Harada, K., Sugawara, I., Ueda, H., Tsuboi, T., and Kitaguchi, T. (2019). Green Fluorescent Protein-Based Glucose Indicators Report Glucose Dynamics in Living Cells. Anal. Chem. *91*, 4821–4830. https://doi.org/10.1021/acs.analchem.9b00447.

56. Mita, M., Sugawara, I., Harada, K., Ito, M., Takizawa, M., Ishida, K., Ueda, H., Kitaguchi, T., and Tsuboi, T. (2022). Development of red genetically encoded biosensor for visualization of intracellular glucose dynamics. Cell Chem. Biol. *29*, 98–108.e4. https://doi.org/10.1016/j.chembiol.2021.06.002.

57. Keller, J.P., Marvin, J.S., Lacin, H., Lemon, W.C., Shea, J., Kim, S., Lee, R.T., Koyama, M., Keller, P.J., and Looger, L.L. (2021). In vivo glucose imaging in multiple model organisms with an engineered single-wavelength sensor. Cell Rep. *35*, 109284. https://doi.org/10.1016/j.celrep.2021.109284.

58. Diaz-Garcia, C.M., Lahmann, C., Martinez-Francois, J.R., Li, B., Koveal, D., Nathwani, N., Rahman, M., Keller, J.P., Marvin, J.S., Looger, L.L., and Yellen, G. (2019). Quantitative in vivo imaging of neuronal glucose concentrations with a genetically encoded fluorescence lifetime sensor. J. Neurosci. Res. *97*, 946–960. https://doi.org/10.1002/jnr.24433.

59. Fehr, M., Frommer, W.B., and Lalonde, S. (2002). Visualization of maltose uptake in living yeast cells by fluorescent nanosensors. Proc. Natl. Acad. Sci. USA *99*, 9846–9851. https://doi.org/10.1073/pnas.142089199.

60. Marvin, J.S., Schreiter, E.R., Echevarría, I.M., and Looger, L.L. (2011). A genetically encoded, high-signal-to-noise maltose sensor. Proteins *79*, 3025–3036. https://doi.org/10.1002/prot.23118.

61. Lager, I., Fehr, M., Frommer, W.B., and Lalonde, S. (2003). Development of a fluorescent nanosensor for ribose. FEBS Lett. *553*, 85–89.

62. Koberstein, J.N., Stewart, M.L., Smith, C.B., Tarasov, A.I., Ashcroft, F.M., Stork, P.J.S., and Goodman, R.H. (2022). Monitoring glycolytic dynamics in single cells using a fluorescent biosensor for fructose 1,6-bisphosphate. Proc. Natl. Acad. Sci. USA *119*, e2204407119. https://doi.org/10.1073/pnas.2204407119.

63. San Martin, A., Ceballo, S., Baeza-Lehnert, F., Lerchundi, R., Valdebenito, R., Contreras-Baeza, Y., Alegria, K., and Barros, L.F. (2014). Imaging Mitochondrial Flux in Single Cells with a FRET Sensor for Pyruvate. PLoS One *9*, e85780. https://doi.org/10.1371/journal.pone.0085780.

64. Bulusu, V., Prior, N., Snaebjornsson, M.T., Kuehne, A., Sonnen, K.F., Kress, J., Stein, F., Schultz, C., Sauer, U., and Aulehla, A. (2017). Spatiotemporal analysis of a glycolytic activity gradient linked to mouse embryo mesoderm development. Dev. Cell *40*, 331–341.e4. https://doi.org/10.1016/j.devcel.2017.01.015.

65. Harada, K., Chihara, T., Hayasaka, Y., Mita, M., Takizawa, M., Ishida, K., Arai, M., Tsuno, S., Matsumoto, M., Ishihara, T., et al. (2020). Green fluorescent protein-based lactate and pyruvate indicators suitable for biochemical assays and live cell imaging. Sci. Rep. *10*, 19562. https://doi.org/10.1038/s41598-020-76440-4.

66. San Martin, A., Ceballo, S., Ruminot, I., Lerchundi, R., Frommer, W.B., and Barros, L.F. (2013). A genetically encoded FRET lactate sensor and its use to detect the Warburg effect in single cancer cells. PLoS One *8*, e57712. https://doi.org/10.1371/journal.pone.0057712.

67. Xu, X., Xu, R., Hou, S., Kang, Z., Lü, C., Wang, Q., Zhang, W., Wang, X., Xu, P., Gao, C., and Ma, C. (2022). A Selective Fluorescent l-Lactate Biosensor Based on an l-Lactate-Specific Transcription Regulator and Forster Resonance Energy Transfer. Biosensors *12*, 1111. https://doi.org/10.3390/bios12121111.

68. Bekdash, R., Quejada, J.R., Ueno, S., Kawano, F., Morikawa, K., Klein, A.D., Matsumoto, K., Lee, T.C., Nakanishi, K., Chalan, A., et al. (2021). GEM-IL: A highly responsive fluorescent lactate indicator. Cell Rep. Methods *1*, 100092. https://doi.org/10.1016/j.crmeth.2021.100092.

69. Aburto, C., Galaz, A., Bernier, A., Sandoval, P.Y., Holtheuer-Gallardo, S., Ruminot, I., Soto-Ojeda, I., Hertenstein, H., Schweizer, J.A., Schirmeier, S., et al. (2022). Single-Fluorophore Indicator to Explore Cellular and Sub-cellular Lactate Dynamics. ACS Sens. *7*, 3278–3286. https://doi.org/10.1021/acssensors.2c00731.

70. Wang, A., Zou, Y., Liu, S., Zhang, X., Li, T., Zhang, L., Wang, R., Xia, Y., Li, X., Zhang, Z., et al. (2024). Comprehensive multiscale analysis of lactate metabolic dynamics in vitro and in vivo using highly responsive biosensors. Nat. Protoc. *19*, 1311–1347. https://doi.org/10.1038/s41596-023-00948-y.

71. Chang, X., Chen, X., Zhang, X., Chen, N., Tang, W., Zhang, Z., Zheng, S., Huang, J., Ji, Y., Zhao, Y., et al. (2024). A bright red fluorescent genetically encoded sensor for lactate imaging. Biochem. Biophys. Res. Commun. *734*, 150449. https://doi.org/10.1016/j.bbrc.2024.150449.

72. Nasu, Y., Murphy-Royal, C., Wen, Y., Haidey, J.N., Molina, R.S., Aggarwal, A., Zhang, S., Kamijo, Y., Paquet, M.E., Podgorski, K., et al. (2021). A genetically encoded fluorescent biosensor for extracellular L-lactate. Nat. Commun. *12*, 7058. https://doi.org/10.1038/s41467-021-27332-2.

73. Koveal, D., Rosen, P.C., Meyer, D.J., Díaz-García, C.M., Wang, Y., Cai, L.H., Chou, P.J., Weitz, D.A., and Yellen, G. (2022). A high-throughput multiparameter screen for accelerated development and optimization of soluble genetically encoded fluorescent biosensors. Nat. Commun. *13*, 2919. https://doi.org/10.1038/s41467-022-30685-x.

74. Bittner, C.X., Loaiza, A., Ruminot, I., Larenas, V., Sotelo-Hitschfeld, T., Gutiérrez, R., Córdova, A., Valdebenito, R., Frommer, W.B., and Barros, L.F. (2010). High resolution measurement of the glycolytic rate. Front Neuroenergetics *2*. Front. Neuroenergetics *2*, 26. https://doi.org/10.3389/fnene.2010.00026.

75. Hou, B.H., Takanaga, H., Grossmann, G., Chen, L.Q., Qu, X.Q., Jones, A.M., Lalonde, S., Schweissgut, O., Wiechert, W., and Frommer, W.B.

(2011). Optical sensors for monitoring dynamic changes of intracellular metabolite levels in mammalian cells. Nat. Protoc. *6*, 1818–1833. https://doi.org/10.1038/nprot.2011.392.

76. Kondo, H., Ratcliffe, C.D.H., Hooper, S., Ellis, J., MacRae, J.I., Hennequart, M., Dunsby, C.W., Anderson, K.I., and Sahai, E. (2021). Single-cell resolved imaging reveals intra-tumor heterogeneity in glycolysis, transitions between metabolic states, and their regulatory mechanisms. Cell Rep. *34*, 108750. https://doi.org/10.1016/j.celrep.2021.108750.
77. Ruminot, I., Schmälzle, J., Leyton, B., Barros, L.F., and Deitmer, J.W. (2019). Tight coupling of astrocyte energy metabolism to synaptic activity revealed by genetically encoded FRET nanosensors in hippocampal tissue. J. Cereb. Blood Flow Metab. *39*, 513–523. https://doi.org/10.1177/0271678X17737012.
78. Kshitiz, Afzal, J., Suhail, Y., Chang, H., Hubbi, M.E., Hamidzadeh, A., Goyal, R., Liu, Y., Sun, P., Nicoli, S., et al. (2022). Lactate-dependent chaperone-mediated autophagy induces oscillatory HIF-1alpha activity promoting proliferation of hypoxic cells. Cell Syst. *13*, 1048–1064.e1047. https://doi.org/10.1016/j.cels.2022.11.003.
79. Xu, D., Vincent, A., González-Gutiérrez, A., Aleyakpo, B., Anoar, S., Giblin, A., Atilano, M.L., Adams, M., Shen, D., Thoeng, A., et al. (2023). A monocarboxylate transporter rescues frontotemporal dementia and Alzheimer's disease models. PLoS Genet. *19*, e1010893. https://doi.org/10.1371/journal.pgen.1010893.
80. Diaz-Garcia, C.M., Meyer, D.J., Nathwani, N., Rahman, M., Martinez-Francois, J.R., and Yellen, G. (2021). The distinct roles of calcium in rapid control of neuronal glycolysis and the tricarboxylic acid cycle. Elife *10*, e64821. https://doi.org/10.7554/eLife.64821.
81. Arce-Molina, R., Cortes-Molina, F., Sandoval, P.Y., Galaz, A., Alegria, K., Schirmeier, S., Barros, L.F., and San Martin, A. (2020). A highly responsive pyruvate sensor reveals pathway-regulatory role of the mitochondrial pyruvate carrier MPC. Elife *9*, e53917. https://doi.org/10.7554/eLife.53917.
82. Lee, H.W., Xu, Y., Zhu, X., Jang, C., Choi, W., Bae, H., Wang, W., He, L., Jin, S.W., Arany, Z., and Simons, M. (2022). Endothelium-derived lactate is required for pericyte function and blood-brain barrier maintenance. EMBO J. *41*, e109890. https://doi.org/10.15252/embj.2021109890.
83. Zaborska, K.E., Dadi, P.K., Dickerson, M.T., Nakhe, A.Y., Thorson, A.S., Schaub, C.M., Graff, S.M., Stanley, J.E., Kondapavuluru, R.S., Denton, J.S., and Jacobson, D.A. (2020). Lactate activation of alpha-cell K(ATP) channels inhibits glucagon secretion by hyperpolarizing the membrane potential and reducing Ca(2+) entry. Mol. Metab. *42*, 101056. https://doi.org/10.1016/j.molmet.2020.101056.
84. Jia, M., Yue, X., Sun, W., Zhou, Q., Chang, C., Gong, W., Feng, J., Li, X., Zhan, R., Mo, K., et al. (2023). ULK1-mediated metabolic reprogramming regulates Vps34 lipid kinase activity by its lactylation. Sci. Adv. *9*, eadg4993. https://doi.org/10.1126/sciadv.adg4993.
85. Dou, X., Fu, Q., Long, Q., Liu, S., Zou, Y., Fu, D., Xu, Q., Jiang, Z., Ren, X., Zhang, G., et al. (2023). PDK4-dependent hypercatabolism and lactate production of senescent cells promotes cancer malignancy. Nat. Metab. *5*, 1887–1910. https://doi.org/10.1038/s42255-023-00912-w.
86. Chen, N., Sun, G., Yuan, X., Hou, J., Wu, Q., Soromou, L.W., and Feng, H. (2014). Inhibition of lung inflammatory responses by bornyl acetate is correlated with regulation of myeloperoxidase activity. J. Surg. Res. *186*, 436–445. https://doi.org/10.1016/j.jss.2013.09.003.
87. Brooks, G.A. (2018). The science and translation of lactate shuttle theory. Cell Metab. *27*, 757–785. https://doi.org/10.1016/j.cmet.2018.03.008.
88. Cantor, J.R., Abu-Remaileh, M., Kanarek, N., Freinkman, E., Gao, X., Louissaint, A., Jr., Lewis, C.A., and Sabatini, D.M. (2017). Physiologic Medium Rewires Cellular Metabolism and Reveals Uric Acid as an Endogenous Inhibitor of UMP Synthase. Cell *169*, 258–272.e17. https://doi.org/10.1016/j.cell.2017.03.023.
89. Zou, Y., Wang, A., Shi, M., Chen, X., Liu, R., Li, T., Zhang, C., Zhang, Z., Zhu, L., Ju, Z., et al. (2018). Analysis of redox landscapes and dynamics in living cells and in vivo using genetically encoded fluorescent sensors. Nat. Protoc. *13*, 2362–2386.
90. Futsaether, C.M., Kjeldstad, B., and Johnsson, A. (1993). Measurement of the intracellular pH of Propionibacterium acnes: comparison between the fluorescent probe BCECF and 31P-NMR spectroscopy. Can. J. Microbiol. *39*, 180–186. https://doi.org/10.1139/m93-025.
91. Zhao, Y., Hu, Q., Cheng, F., Su, N., Wang, A., Zou, Y., Hu, H., Chen, X., Zhou, H.M., Huang, X., et al. (2015). SoNar, a highly responsive NAD+/NADH sensor, allows high-throughput metabolic screening of anti-tumor agents. Cell Metab. *21*, 777–789.
92. Zhao, Y., Wang, A., Zou, Y., Su, N., Loscalzo, J., and Yang, Y. (2016). In vivo monitoring of cellular energy metabolism using SoNar, a highly responsive sensor for NAD(+)/NADH redox state. Nat. Protoc. *11*, 1345–1359.
93. Tantama, M., Hung, Y.P., and Yellen, G. (2011). Imaging intracellular pH in live cells with a genetically encoded red fluorescent protein sensor. J. Am. Chem. Soc. *133*, 10034–10037. https://doi.org/10.1021/ja202902d.
94. Wu, D., Harrison, D.L., Szasz, T., Yeh, C.-F., Shentu, T.-P., Meliton, A., Huang, R.-T., Zhou, Z., Mutlu, G.M., Huang, J., and Fang, Y. (2021). Single-cell metabolic imaging reveals a SLC2A3-dependent glycolytic burst in motile endothelial cells. Nat. Metab. *3*, 714–727. https://doi.org/10.1038/s42255-021-00390-y.
95. Zhang, J., Chen, F., Tian, Y., Xu, W., Zhu, Q., Li, Z., Qiu, L., Lu, X., Peng, B., Liu, X., et al. (2023). PARylated PDHE1alpha generates acetyl-CoA for local chromatin acetylation and DNA damage repair. Nat. Struct. Mol. Biol. *30*, 1719–1734. https://doi.org/10.1038/s41594-023-01107-3.
96. Cai, X., Ng, C.P., Jones, O., Fung, T.S., Ryu, K.W., Li, D., and Thompson, C.B. (2023). Lactate activates the mitochondrial electron transport chain independently of its metabolism. Mol. Cell *83*, 3904–3920.e7. https://doi.org/10.1016/j.molcel.2023.09.034.
97. Wollman, A.J.M., Kioumourtzoglou, D., Ward, R., Gould, G.W., and Bryant, N.J. (2022). Large scale, single-cell FRET-based glucose uptake measurements within heterogeneous populations. iScience *25*, 104023. https://doi.org/10.1016/j.isci.2022.104023.
98. Hao, X., Gu, H., Chen, C., Huang, D., Zhao, Y., Xie, L., Zou, Y., Shu, H.S., Zhang, Y., He, X., et al. (2019). Metabolic Imaging Reveals a Unique Preference of Symmetric Cell Division and Homing of Leukemia-Initiating Cells in an Endosteal Niche. Cell Metab. *29*, 950–965.e6. https://doi.org/10.1016/j.cmet.2018.11.013.
99. Machler, P., Wyss, M.T., Elsayed, M., Stobart, J., Gutierrez, R., von Faber-Castell, A., Kaelin, V., Zuend, M., San Martin, A., Romero-Gomez, I., et al. (2016). In Vivo Evidence for a Lactate Gradient from Astrocytes to Neurons. Cell Metab. *23*, 94–102. https://doi.org/10.1016/j.cmet.2015.10.010.
100. Diaz-Garcia, C.M., Mongeon, R., Lahmann, C., Koveal, D., Zucker, H., and Yellen, G. (2017). Neuronal Stimulation Triggers Neuronal Glycolysis and Not Lactate Uptake. Cell Metab. *26*, 361–374. https://doi.org/10.1016/j.cmet.2017.06.021.
101. Wolfe, A.D., Koberstein, J.N., Smith, C.B., Stewart, M.L., Gonzalez, I.J., Hammarlund, M., Hyman, A.A., Stork, P.J.S., Goodman, R.H., and Colón-Ramos, D.A. (2024). Local and dynamic regulation of neuronal glycolysis in vivo. Proc. Natl. Acad. Sci. USA *121*, e2314699121. https://doi.org/10.1073/pnas.2314699121.
102. Lin, C., Liu, L., and Zou, P. (2023). Functional imaging-guided cell selection for evolving genetically encoded fluorescent indicators. Cell Rep. Methods *3*, 100544. https://doi.org/10.1016/j.crmeth.2023.100544.
103. Unger, E.K., Keller, J.P., Altermatt, M., Liang, R., Matsui, A., Dong, C., Hon, O.J., Yao, Z., Sun, J., Banala, S., et al. (2020). Directed Evolution of a Selective and Sensitive Serotonin Sensor via Machine Learning. Cell *183*, 1986–2002.e26. https://doi.org/10.1016/j.cell.2020.11.040.
104. Biswas, S., Khimulya, G., Alley, E.C., Esvelt, K.M., and Church, G.M. (2021). Low-N protein engineering with data-efficient deep learning. Nat. Methods *18*, 389–396. https://doi.org/10.1038/s41592-021-01100-y.

105. McMahon, S.M., and Jackson, M.B. (2018). An Inconvenient Truth: Calcium Sensors Are Calcium Buffers. Trends Neurosci. *41*, 880–884. https://doi.org/10.1016/j.tins.2018.09.005.

106. Sun, H., Zhang, Z., Li, T., Li, T., Chen, W., Pan, T., Fang, S., Liu, C., Zhang, Y., Wang, L., et al. (2023). Live-cell imaging reveals redox metabolic reprogramming during zygotic genome activation. J. Cell. Physiol. *238*, 2039–2049. https://doi.org/10.1002/jcp.31054.

107. Harrison, D., Wu, D., Huang, J., and Fang, Y. (2021). Single-cell lactate production rate as a measure of glycolysis in endothelial cells. STAR Protoc. *2*, 100807. https://doi.org/10.1016/j.xpro.2021.100807.